Accepted version

Original Publication:

Flôres DEFL, Oda GA. Quantitative Study of Dual Circadian Oscillator Models under Different Skeleton Photoperiods. J Biol Rhythms. 2020 Feb 4:748730420901939.
 doi: 10.1177/0748730420901939. [Epub ahead of print]

Article type
Original Research

Corresponding author info:

Gisele Akemi Oda

Universidade de São Paulo. Rua do Matão, Travessa 14, nº 321, Cidade Universitaria. Departamento de Fisiologia, sala 321

05508-900 - São Paulo - SP - Brazil

Phone: +55 11 30917480

E-mail address: gaoda@ib.usp.br

Article Title

Quantitative study of dual circadian oscillator models under different skeleton photoperiods

Short Title:

Dual-oscillator models under skeleton photoperiods

Authors

Danilo Eugênio de França Laurindo Flôres

Gisele Akemi Oda

Affiliation

Instituto de Biociências, Universidade de São Paulo, Sao Paulo, Brazil

ABSTRACT

The daily proportion of light and dark hours (photoperiod) changes annually and plays an important role in the synchronization of seasonal biological phenomena, such as reproduction, hibernation and migration. In mammals, the first step of photoperiod transduction occurs in the suprachiasmatic nuclei (SCN), the circadian pacemaker that also coordinates 24h activity rhythms. Thus, in parallel with its role in annual synchronization, photoperiod variation acutely shapes day/night activity patterns which vary throughout the year. Systematic studies of this behavioral modulation help understand the mechanisms behind its transduction at the SCN level. To explain how entrainment mechanisms could account for daily activity patterns under different photoperiods, Colin Pittendrigh and Serge Daan proposed a conceptual model in which the pacemaker would be composed of two coupled, Evening (E) and Morning (M) oscillators. Although the E-M model exists for more than 40 years now, its physiological bases are still not fully resolved and it has not been tested quantitatively under different photoperiods. To better explore the implications of the E-M model we performed computer simulations of two coupled limit-cycle oscillators. Four model configurations were exposed to systematic variation of skeleton photoperiods, and the resulting daily activity patterns were assessed. The criteria for evaluating different model configurations was the successful reproduction of two key behavioral phenomena observed experimentally: activity psi-jumps and photoperiod induced changes in activity phase duration. We compared configurations with either separate light inputs to E and M or the same light inputs to both oscillators. The former replicated experimental results closely, indicating that the configuration with separate E and M light inputs is the mechanism that best reproduces the effects of different skeleton photoperiods on day/night activity patterns. We hope this model can contribute to the search for E and M and their light input organization in the SCN.

INTRODUCTION

Natural environments undergo cyclic seasonal changes in biotic and abiotic factors throughout the year. Accordingly, organisms have evolved seasonal adjustments in physiology and behavior associated to these changes (Baker, 1938), such as the seasonal reproduction, migration and hibernation. Synchronization of these seasonal phenomena is attained by diverse annual environmental cues that serve as natural calendars. One of these cues is photoperiod, the daily proportion between light and dark hours within the 24-hour light/dark cycle (Bradshaw and Holzapfel, 2007) (Fig. 1A top). Thus, given the regularity of photoperiodic changes that recur from year to year, many organisms have evolved the ability to interpret photoperiod and use it as a highly reliable anticipatory cue for future seasonal conditions (Bradshaw and Holzapfel, 2007).

In addition to its role as seasonal synchronizer, photoperiod variation also has profound effects on the day/night patterns of activity on a 24-hour scale (Pittendrigh, 1988). As reported in different species, two parameters of daily activity are modified along with the day-to-day changes in photoperiod: activity duration (time between daily activity onset and offset, **α**) and its phase of entrainment (time between a reference phase in the light/dark cycle and a reference phase in the activity rhythm, **ψ**). For instance, in day-active (diurnal) animals, **α** lasts longer during spring/summer than on winter/autumn days. This has been reported in different vertebrate species exposed to natural photoperiods, for example, grizzly bears (Ware et al., 2012), squirrels (Wauters et al., 1992; Williams et al., 2012), birds (Daan and Aschoff, 1975) and humans as inferred from sleep duration (de la Iglesia et al., 2015; Yetish et al., 2015). The inverse is observed for night-active (nocturnal) animals, which present a shorter activity phase in the spring/summer, as reported for a few rodents (Boulos and Macchi, 2005; Daan and Aschoff, 1975; Kenagy, 1976) and bats (Erkert, 2000). Representative data from a nocturnal rodent in Figure 1A illustrate the photoperiod-dependent changes in **α** (Daan and Aschoff, 1975).

As for **ψ,** it is remarkably fixed when photoperiod is varied in the vicinity of LD12:12, as shown in data from hamsters in Figure 1C in the interval LD9:15 to LD15:9. Activity onset occurs shortly after

lights-off, independent of photoperiod. The same has been observed in flying squirrels (DeCoursey, 1972). For these and other nocturnal animals, this means that activity onset is locked to dusk, whatever the timing of dusk throughout the seasons; this is an adaptive strategy from the ecological point of view (Pittendrigh and Daan, 1976a). However, experiments with systematic photoperiod manipulation have shown that the tight phase-association between activity onset and dusk is lost under extreme, long or short days (Elliott, 1976). This is illustrated in the extreme values of Figure 1C. Our aim is to understand complex response patterns such as the abrupt phase changes and $\boldsymbol{\alpha}$ modulations displayed in Figure 1, using mathematical modeling and computer simulations. Our simple model is based on physiological and anatomical knowledge of the circadian system that has been accumulated over decades. Our objective is to indicate minimum elements of this system that are sufficient to process the length of the day throughout the year.

In mammals, a circadian oscillator located in the hypothalamic suprachiasmatic nuclei (SCN) has a dual role in mediating the photoperiodic transduction on physiology and behavior (Coomans et al., 2015; Goldman, 2001). On one hand, it generates daily activity rhythms in behavior that display photoperiod-dependent patterns, as indicated above. On the other hand, it shapes photoperiod-dependent melatonin profiles that relay time-of-year information to the hypothalamus-hypophyseal axis for control of seasonal phenomena (Ikegami and Yoshimura, 2012; Illnerová and Vaněček, 1982). These two functions are achieved through a reorganization of the SCN internal structure as the photoperiod changes (Buijink et al., 2016; Ciarleglio et al., 2011; Evans et al., 2013; Mrugala et al., 2000; Schwartz et al., 2001; Sumová et al., 1995; Tackenberg and McMahon, 2018; VanderLeest et al., 2007). While the first function evokes day-to-day responses on activity patterns, the second allows anticipatory initiation of cascades of developmental and reproductive processes that culminate in seasonal events distant in time. In this work, we focus on the first function and pursue how daily locomotor activity is affected by different photoperiods.

In the 24-hour time scale, the circadian oscillator/pacemaker in the SCN is entrained by the daily light/dark cycle, via direct neuronal inputs from the retina (Abrahamson and Moore, 2001). To explain how this entrainment mechanism could account for daily activity patterns under different photoperiods,

Pittendrigh and Daan (1976a) proposed that the pacemaker could be composed of two coupled oscillators. The oscillators have been named "evening" (E) and "morning" (M). The authors proposed that this qualitative dual-oscillator model could potentially account for photoperiodic changes in **α** if one oscillator tracked dawn (M) and the other tracked dusk (E), changing the phase relationship to one another throughout the year.

Although the E-M model exists for more than 40 years, its physiological bases are still not fully resolved (Daan et al., 2001; Helfrich-Förster, 2009; Inagaki et al., 2007; Yoshikawa et al., 2017) and it has not been quantitatively tested under varying photoperiods using mathematical models. For instance, it is still not clear, to what extent two SCN components separately entrained by dawn and dusk are necessarily required for photoperiod encoding, both from the physiological and from the dynamical points of view.

To better explore this proposition, previous studies have recorded daily activity rhythms of rodents exposed to **skeleton photoperiods** (Pittendrigh and Daan, 1976b; Spoelstra et al., 2014). Instead of a full light/dark cycle, this protocol consists of two light pulses given at the times corresponding to the transitions between the light and dark phases of the full cycle (Fig. 1B top). Therefore, photoperiod is modelled as the ratio of the two intervals between a "dawn" and a "dusk" light pulses. Despite the simplicity of skeleton photoperiods, they are sufficient to i) adjust reproductive function according to the seasons (Milette and Turek, 1986; Wade et al., 1986) and ii) induce daily changes in **α** according to photoperiod (Pittendrigh and Daan, 1976b; Spoelstra et al., 2014; Takahashi and Menaker, 1982).

When exposed to skeleton photoperiods animals always concentrate daily activity in one of the darkness intervals between light pulses, which is assigned the "night interval" for nocturnal species. Whether activity occurs in the longer or the shorter interval between pulses depends on previous light conditions and on the relative lengths of the intervals. Curiously, for nocturnal animals, when **α** is gradually compressed by reducing the current night interval, the activity phase eventually shifts to the complementary interval, thus inverting the day and night references of the cycle (Fig. 1B). This inversion of the phase of entrainment **ψ** (psi), is denoted **psi-jump** (Pittendrigh and Daan, 1976b). Critically, before

the psi-jump, the activity phase tracks one pulse of the skeleton photoperiod and, afterwards, it tracks the opposite pulse (Fig. 1B).

Modeling efforts have been made before to understand E and M dynamics in constant conditions (Daan and Berde, 1978; Kawato and Suzuki, 1980; Oda and Friesen, 2002; Oda et al., 2000). Other studies have modelled entrainment of a single oscillator (Pittendrigh and Daan, 1976a; Schmal et al., 2015) or very complex oscillator networks (Taylor et al., 2016) under different photoperiods. In the present study we simulate a system of two coupled limit-cycle oscillators under skeleton photoperiod manipulations and seek minimal configurations that could display photoperiod dependent **α** compression and **psi-jump.** To our knowledge this is the first attempt to explicitly model E and M dynamics in the context of photoperiodism.

MATERIAL AND METHODS

To investigate the effects of photoperiod on the E-M model, we used two coupled non-linear limit-cycle oscillators, governed by the Pittendrigh-Pavlidis equations. These equations have been previously used to model circadian rhythms in *Drosophila* (Pittendrigh, 1981; Pittendrigh et al., 1991) and the E and M oscillators in rodents (Oda and Friesen, 2002; Oda et al., 2000). Each oscillator is described by a set of two equations (1-4). Following previous conventions (Oda et al., 2000), the terms from E and M oscillators are identified by subscribed letters.

Evening oscillator (E):

$$dR_E/dt = R_E - c_E S_E - b_E S_E^2 + (d_E - L) + K \quad (1)$$

$$dS_E/dt = R_E - a_E S_E + C_{ME} S_M \quad (2)$$

Morning oscillator (M):

$$dR_M/dt = R_M - c_M S_M - b_M S_M^2 + (d_M - L) + K \quad (3)$$

$$dS_M/dt = R_M - a_M S_M + C_{EM} S_E \quad (4)$$

State variables R and S together describe the state of one oscillator at a given time point. The R variable is prevented from reaching negative values. Parameters a, b, c and d are set to fixed values and collectively define an oscillator configuration, with intrinsic period and amplitude. K (Kyner) is a small nonlinear term that guarantees numerical smoothness ($K=k_1/(1 + k_2R^2)$, $k_1=1$, $k_2=100$) (Oda et al., 2000). The L term simulates the light input (forcing variable). Its value is maintained at zero to simulate the dark hours. When lights are turned on, it is changed to a positive amplitude value in arbitrary units (a.u.), which simulates the light intensity. In one particular case indicated below, we used pulses of negative amplitude. The coupling term C controls the strength with which the E oscillator influences the morning oscillator (C_{EM}) and vice-versa (C_{ME}). When coupling is symmetric, $C_{EM} = C_{ME}$.

In most cases, we used a standard configuration (a=0.85, b=0.3, c=0.8, d=0.5), previously employed to model circadian rhythms in rodents (Oda et al., 2000). Other configurations have been explored to investigate the dependence of phenomena on the period and amplitude of oscillators (Supplemental Section). Computer simulations were performed in the *CircadianDynamix* extension of the *Neurodynamix II* software (Friesen and Friesen, 1994) using the Euler method for numerical integration, with 1000 integration steps per 24 hours.

In our simulations we portray the phases of the circadian oscillators (squares and triangles) and of the behavioral rest/activity rhythm (black bars) separately (Fig. 2), to emphasize the temporal interdependence between oscillator and behavioral activity. In Figure 2, we explicitly show how the phases corresponding to activity were transduced from the phases of the circadian oscillator. This was achieved by defining a threshold, which was set to 40% of the state variable amplitude. Whenever the S variable of either oscillator went above its threshold, the model organism was considered as resting (activity was inhibited), otherwise, it was considered as active. Thus, in the dual oscillator model, the total activity band was determined by E and M together (Fig. 2), with activity set in antiphase to the peak amplitude of the circadian oscillators. This is equivalent to the phase relationship between behavioral activity and peak SCN electrical discharge in nocturnal mammals (Houben et al., 2009).

Finally an extra step was added in the simulations to better fit experimental data for nocturnal animals under skeleton photoperiods. The composite phases of oscillators and activity were delayed in five hours

throughout all simulations, establishing an interval lag relative to the light signal. Importantly, we maintained the same fixed phase relationship between oscillators and activity rhythm (Fig. 2). This step was necessary because although activity patterns in the simulations matched closely to experimental data, there was a discrepancy between the exact time of their occurrences. This discrepancy was resolved by setting a phase difference between the light pulses and the simulated oscillator.

The daily light/dark cycle was modelled as a skeleton photoperiod, with two light pulses every 24 hours (Fig. 1B top) (Pittendrigh and Daan, 1976b; Spoelstra et al., 2014). We simulated four configurations of the model to represent different putative physiological mechanisms (Fig. 3 top). As a control, in Model I we first simulated a single oscillator subjected to the skeleton photoperiod (isolated E, with null coupling) (Fig. 3A top). The remaining configurations all had both E and M oscillators, with symmetric coupling. In Model II, each of the two pulses of the skeleton photoperiod was applied to only one of the oscillators (Fig. 3B top). In Model III, both pulses were applied to both oscillators (Fig. 3C top). Finally, in Model IV the M oscillator received pulses with negative amplitude (Fig. 3D top).

A model where one oscillator receives light input and the other does not was not considered, because the light-insensitive oscillator would just passively follow the phase of the sensitive one, with negligible changes in phase-relationship.

The four configurations of the model were exposed to different skeleton photoperiods, with different intervals between the daily light pulses. Intervals were reduced from 22 to 2 hours, in 2-hour steps applied sequentially, each for 15 days. Importantly, this 15-day interval ensures end of transients and that the entrainment phase achieved by the circadian oscillator is the steady state one for each different photoperiod. The lengths of the intervals were measured from the beginning of the first pulse to the beginning of the second one. On the last day of exposure to each photoperiod, we measured **α** and the phase of entrainment. **α** was measured as the interval between the daily onset and the daily end of activity. The phase of entrainment was measured as the interval between the midpoint of pulses and two reference phases of the rhythm, activity onset and offset, and then converted to the 0-24h circular scale.

SIMULATION RESULTS

We have tested the photoperiodic response of the four putative models. When exposed to different skeleton photoperiods, all configurations of the model are successfully synchronized to 24 hours. Representative actograms are shown in Figure 3A-D (bottom). For the single oscillator in Model I (Fig. 3A), only the E oscillator is simulated. The actogram in Figure 3A (bottom) depicts a daily activity band in black, with the two pulses of the skeleton photoperiod in white and the oscillator variable peaks as empty squares. We assign "dusk" to the pulse which is locked to activity onset and "dawn" to the other pulse. When the "night" interval between pulses is decreased from 22 to 14 hours, the onset of activity remains phase-locked to the dusk pulse. This is summarized in Figure 3E, which shows the phase of entrainment quantified on the last day of exposure to each photoperiod. With a single oscillator, there is no noticeable change in α between photoperiods, as observed in actograms (Fig. 3A bottom) and quantifications (Fig. 3I). When the interval between pulses is decreased to 12 hours, a psi-jump is observed (Fig. 3A bottom) and, from that point onwards, the activity onset follows the dawn pulse of the skeleton photoperiod (Fig. 3A bottom, 3E). In summary, with one oscillator, we can observe the psi-jump phenomenon, but α remains unchanged throughout different photoperiods.

Having observed the behavior of a single oscillator, we can then explore putative E-M mechanisms. In Model II, the actogram depicts the activity band, together with squares and triangles representing E and M state-variable peaks, respectively (Fig. 3B bottom). For simplicity, we chose to model a completely symmetric system in terms of oscillators and coupling, which leads to an overlap between E and M peaks in constant conditions (Fig. 3B bottom), as reported previously (Oda and Friesen, 2002). When the system is exposed to different photoperiods, again, the activity onset is phase-locked to the dusk pulse, up to the 12-hour "night" interval (Fig. 3B bottom, 3F). Furthermore, the E and M peak phases separate from each other upon initiation of the skeleton photoperiods (circles in Fig. 3B bottom) and this becomes more pronounced as the "night" interval between pulses is decreased from 22 to 12 hours (Fig. 3B bottom). Consequently, there is a corresponding decrease in α (Fig. 3B bottom, 3J). When the interval between pulses is further decreased to 10 and then 8 hours, there is a psi-jump (Fig. 3B bottom, 3F). After this, α is gradually increased (Fig. 3J) and the activity onset tracks the opposite, dawn pulse of the skeleton

photoperiod (Fig. 3F). These results indicated that Model II accounts for photoperiod-induced **α** adjustments.

One feature observed experimentally in **α** adjustments is the maintenance of **α** on the first days after an animal is released in constant darkness from a photoperiod protocol (Pittendrigh and Daan, 1976b). We released the oscillators of Model II in constant conditions, after being held in different photoperiods, and observed that **α** was very similar on the first day. Throughout the days in constant conditions, **α** gradually lengthened to a steady-state value (Suppl. Fig. S1).

We then explored variations in the coupling strength between E and M in Model II (Fig. 4). With very weak coupling, each oscillator tracks one of the pulses, following the pulse times almost passively (Fig. 4A). This results in a great modulation of **α** (Fig. 4A). Upon a slightly stronger coupling (Fig. 4B), the oscillators remain closer together in the more extreme photoperiods, with a more stable and larger **α** when the interval between pulses is too long. As the "night" interval between pulses is changed to intermediate photoperiods, E and M separate from each other and **α** is modulated (Fig. 4B). With stronger coupling, higher than the standard value used in Figure 3B, E and M stick together throughout most photoperiods (Fig. 3G, H), initially following the dusk pulse and then shifting to the opposite pulse. Consequently, **α** remains more stable throughout photoperiods. Strikingly, when we compare the weaker coupling with the stronger ones, there is a change in the threshold photoperiod before the psi-jump. With weaker coupling, psi is reversed when the "night" interval between pulses is set to 10 hours (Fig. 4A, B), whereas with higher coupling strengths, psi-jump happens at "night" intervals of 8 and 6 hours (Fig. 4C, D).

The E-M model above is responsive to photoperiod variations, however, it would imply that, in the SCN, distinct subregions corresponding to E and M responded separately to dawn or dusk inputs. Alternatively, it is possible that E and M subregions are equally responsive to dawn and dusk stimuli. To test this hypothesis, in Model III, again we have a completely symmetric set of E and M oscillators, but both oscillators are directly synchronized by both pulses of the skeleton photoperiod (Fig. 3C top). When exposed to the different photoperiods, the E and M phases remained completely overlapped, as seen from the squares and triangles (Fig. 3C bottom). This overlap remained regardless of the interval between

pulses (Fig. 3C bottom). As a result, **α** remained basically unchanged (Fig. 3K). The psi-jump occurred just like in the previous versions of the model (Fig. 3G). In short, a completely symmetric E-M model behaves essentially as the single oscillator, when both E and M are equally responsive to the pulses of the skeleton photoperiod. We then hypothesized that if a phase difference between E and M existed in Model III, it could generate different responses to light. As reported previously (Oda et al., 2000), a phase difference can generate separate responses to single light pulses in a DD background. To this end, simulations were performed with an asymmetric configuration. We used two oscillators with different intrinsic periods (Suppl. Fig. S2A, B), which results in a basal phase difference in constant conditions (Suppl Fig. S2C). Despite this basal phase difference, E and M phases still overlap in the presence of two light inputs in a Model III configuration (Suppl. Fig. S2C, D). As shown in Supplemental Figure S2E, each individual oscillator, when isolated, presents very similar phases of entrainment to the different skeleton photoperiods. This explains why, in the coupled system, the phases of the two oscillators are brought together by the pulses. Thus, Model III does not allow independent E and M shifts that could generate α changes.

The original E-M conceptual model suggested that the component oscillators should have different intrinsic properties, such as period and phase-response to light (Pittendrigh and Daan, 1976b, 1976a). As a result, each component oscillator would phase-lock to a different pulse of the skeleton photoperiod. As the interval between pulses changed with different photoperiods, the oscillators would tend to separate from each other and promote **α** adjustments. In the asymmetric E-M case described above, however, both oscillators tracked the dusk pulse, despite their asymmetries (Suppl. Fig. S2E). In this sense, we hypothesized that a fourth version of the model could be made responsive to photoperiodic variations if we added novel, *specific* asymmetries between E and M, so that each oscillator would track a different pulse of the skeleton photoperiod when isolated.

After several attempts, described in the Supplemental Section (and Suppl. Fig. S3-8), we arrived at Model IV (Fig. 3D top). It is a variation of Model III, in which the M oscillator receives negative pulses. This guarantees that the isolated E and M go to opposite directions when the photoperiod is changed, due to a change in the phase-response to the pulses (Suppl. Fig. S8). When isolated, E behaves as the single

oscillator in Figures 3A and 3E, following the dusk pulse, while M follows the dawn pulse (Suppl. Fig. S8). In the coupled system (Fig. 3D top) the free-running rhythm is again equivalent to E-M Models II and III (Fig. 3D bottom). After exposure to skeleton photoperiods, the E and M activities separate (Fig. 3D bottom). Moreover, the phase-relationship between E and M is adjusted with varying intervals between pulses (Fig. 3D bottom). Hence, there is a change in **α**, especially in photoperiods close to the 12-hour interval (Fig. 3L). As with all previous models, the compound system first tracks one pulse, then there is a psi-jump when the "night" interval is decreased beyond 10 hours, and the system tracks the opposite pulse (Fig. 3H). Altogether, these results indicate that the addition of specific asymmetries can rescue a photoperiodic response in a coupled E-M model in which both oscillators are directly synchronized to both pulses of the skeleton photoperiod.

MODEL LIMITATIONS

Our dual oscillator model, with only two emergent components, has been enough to coordinate our understanding of photoperiod-induced **α** changes and psi-jumps, which are phenomena observed at the behavioral level. However, several experiments at the neural level indicate that the photoperiodic adjustments in the rhythm of the compound nuclei result from the phase-distribution of the rhythms from single SCN cells, or sub-regions composed of groups of cells (Brown and Piggins, 2009; Buijink et al., 2016; Inagaki et al., 2007; Jagota et al., 2000; Naito et al., 2008; Rohling et al., 2006; Schaap et al., 2003; VanderLeest et al., 2007; Yoshikawa et al., 2017). It is likely that E and M correspond to SCN sub-regions, formed by coherent groups of cells. The particular properties of each oscillator may arise not only from variations in intracellular mechanisms (Nuesslein-Hildesheim et al., 2000) but also from differences in intercellular coupling within cell groups (Evans et al., 2013; Farajnia et al., 2014; Lucassen et al., 2012). A model that included changes in single cell and oscillator network properties could certainly contribute to elucidating the explicit mechanisms and refined aspects of photoperiod encoding in multi-oscillatory organs. For example, an *in silico* study on evolving genetic networks suggests that a

greater complexity (more oscillators and interactions) can be advantageous for a proper response to photoperiod when it is accompanied by noise fluctuations in environmental light (Troein et al., 2009).

Different photoperiods impose modifications within the fine structure of circadian oscillators, which persist under constant conditions (Mrugala et al., 2000). For instance, pineal glands from birds, explanted *in vitro,* express melatonin patterns that match the previous photoperiodic conditions experienced by the animals *in vivo* (Brandstätter et al., 2000). In mammals, it has been shown that, unlike the wild-type mice, VIP KO mice fail to display aftereffects of entrainment to different photoperiods (Lucassen et al., 2012). Since VIP is a peptide that promotes inter-neuronal coupling in the SCN, this indicates that cell-to-cell communication is indispensable for endogenous encoding of photoperiodic information. These examples strongly imply that photoperiod coding has long-lasting effects, likely involving coupling reorganization within the cellular population that comprises the circadian clocks. Buijink et al. (2016) report greater period instability in Per2::Luc rhythms of individual cells in the mouse SCN, in long days versus short days, which further indicates a photoperiod-dependent change in coupling strength.

Coupling changes certainly entail oscillator amplitude changes (Oda et al., 2000), which in turn affect the clock Phase Response Curve to light (Lakin-Thomas et al., 1991). The ultimate mechanism behind photoperiod encoding could possibly lie on the seasonal modulation of the clock responses to light inputs (Evans et al., 2004; Pittendrigh et al., 1991). In this sense, the model proposed in the present work could be refined by splitting E and M each into a distinct subpopulation of oscillators and manipulating individual coupling parameters in a complex neuronal network. This strategy was used by Taylor et al. (2016) to model different regions of the SCN and they found a mild photoperiodic modulation in the phase difference between the regions. In their case, however, only one region received light inputs, which may explain the lack of pronounced photoperiodic effects.

Finally, our models do not consider the interaction of a homeostatic sleep drive and a circadian oscillator (Borbély et al., 2016; Deboer, 2018) in determining activity onsets and offsets under different photoperiods. Although prior activity is known to affect sleep propensity, several studies indicate that the timing of sleep under different photoperiods is more strongly determined by the circadian pacemaker. In rats, sleep deprivation under different photoperiods is compensated on the next day by different sleep

compositions, with little change in sleep timing (Franken et al., 1995). In Borbély and Neuhaus (1978), the timing of sleep and wake onsets on the first day of abrupt photoperiod change is still shaped by the photoperiod of the previous day. Trachsel et al. (1986) have shown that this also happens in rats released into constant darkness. We recognize that a sleep homeostat could potentially refine timing of activity. Thus, the model could be further complemented by the addition of a homeostatic oscillator. But we would still consider a system composed by 2 coupled circadian oscillators to explain the complex dynamics of activity onsets and offsets in different light conditions.

DISCUSSION

From an ecological viewpoint, it is tempting to interpret that the duration of daily activity in different seasons is a direct response of organisms to the availability of favorable conditions for activity along the 24 hours (Bennie et al., 2014). For instance, compression of daily activity in diurnal organisms during autumn/winter can be viewed simply as a reaction to fewer available light hours or to the concentration of warm temperatures around noon. However, laboratory studies with photoperiod manipulations have established that seasonal variation in $\boldsymbol{\alpha}$ has an endogenous component, as shown by the establishment of non-linear $\boldsymbol{\alpha}$ and $\boldsymbol{\psi}$ variations when photoperiod is varied linearly (Fig. 1B, C) (Elliott, 1976). Understanding the mechanisms of photoperiod dependence in $\boldsymbol{\alpha}$ and $\boldsymbol{\psi}$ has still been a challenge, requiring mathematical modeling. It has been proposed that, in mammals, photoperiod variations of daily activity patterns involve (at least) two oscillators, E and M, which control activity onset and offset, and are differentially entrained by dawn and dusk (Pittendrigh and Daan, 1976a).

In the mammalian circadian system, the SCN mediates photoperiodic adjustments in activity $\boldsymbol{\alpha}$, therefore, the nuclei have been strong candidates for the physical substrate of the E and M oscillators (Daan et al., 2001; Helfrich-Förster, 2009). The SCN function as an overt oscillatory unit, expressing a 24-hour profile in multi-unit electrical activity (Houben et al., 2009). The duration of this high electrical activity state depends on the length of the photophase (reviewed in Coomans et al., 2015) and is mirrored

in the daily **α duration** of overt activity rhythms (Houben et al., 2009) and melatonin profiles (Illnerová and Vaněček, 1982).

Our quantitative analysis of putative E-M models is an attempt to elucidate the requirements of the dual-oscillator system, which allow a response to different photoperiods. The general model predictions should be valid, irrespective of the precise tissue/cellular correspondence, as long as E and M behave as limit-cycle oscillators. In the current study, we searched for model configurations that presented the experimentally observed responses to (skeleton) photoperiods (Fig. 1B). After changes in the interval between pulses, a successful model should present i) photoperiod-driven adjustments in **α**, with one oscillator tracking dawn and the other tracking dusk, and ii) a psi-jump after the inter-pulse interval reached a threshold duration.

One emergent feature of all simulations is that when two light pulses are applied per day, the phase of the oscillator system tracks one of the pulses and remains this way upon systematic changes in the interval between pulses, until a certain threshold value. After this threshold it tracks the other pulse and the transition of these two regimes occurs abruptly, resulting in a psi-jump. This is true for a one or two-oscillator system and independent of the configurations that were tested (Fig. 3E-H). The switch in the pulse association is typical of models with two zeitgeber inputs when the phase difference between them is systematically varied (Oda and Friesen, 2011) and it illustrates the contribution of mathematical modeling in coordinating our interpretation of complex dynamical phenomena. The two-zeitgeber model configuration also predicted that bistability phenomena would occur when the two zeitgebers attained the vicinity of an anti-phase relationship. This is in fact observed when skeleton photoperiods are systematically varied and the light pulses attain intervals around 12h, when the "night interval" chosen by the nocturnal individual depends on the previous phase of activity (Pittendrigh and Daan, 1976b; Takahashi and Menaker, 1982).

While psi-jumps are easily replicated, photoperiod-driven adjustments in **α** appeared more challenging. In the simplest configuration, Model I, a single oscillator presented no considerable change in **α**. Model II, on the other hand, expressed photoperiod modulation of **α**. In this model, the coupling strength between oscillators determined how independently they "moved" under different photoperiods.

In a loosely coupled system, the oscillators were almost independent from each other (Fig. 4A), passively following dawn and dusk. Therefore, Model II was able to replicate photoperiod-induced changes in **α** especially with low to mid coupling strengths (Fig. 4A, B). Interestingly, these **α** changes persisted when the simulated light pulses were turned-off, mimicking photoperiod aftereffects on **α** (Fig. S1). However, the aftereffects persist for a short time, up to 8 days, depending on the initial value. The quick **α** decompression likely happens because our model is not including coupling changes in different photoperiods, which may enhance the aftereffects (Lucassen et al., 2012). But it is all the more striking to show that, even without these internal coupling changes, photoperiod aftereffects on **α** can be simulated in Model II.

Despite the success of Model II in replicating experimental results, to our knowledge, there has not been any evidence yet that specific SCN subpopulations receive dawn-only- or dusk-only-signals from its neuronal inputs. Signals from the retina reach the SCN through direct retinohypothalamic (Abrahamson and Moore, 2001) and indirect geniculohypothalamic (Jacob et al., 1999) pathways. In the former, light signals are conveyed by glutamatergic synapses that stimulate vasoactive intestinal peptide (VIP)-containing neurons (Jones et al., 2018). In the indirect geniculohypothalamic pathway, neuropeptide Y (NPY) projections from the intergeniculate leaflet (IGL) input zeitgeber information to the SCN (Harrington et al., 1985). This pathway has been previously associated to photoperiodic responses. IGL-NPY signals have been implicated in entrainment of activity rhythms to fixed skeleton photoperiods (Edelstein and Amir, 1999), to complete photoperiods (Freeman et al., 2004; Kim and Harrington, 2008) and in the photoperiodic adjustments in the SCN (Menet et al., 2001). Moreover, NPY levels are crepuscular in the rat SCN (Shinohara et al., 1993) and the peptide has been shown to interfere with phase-shifts *in vivo* (Weber and Rea, 1997) and in the SCN *in vitro* (Biello et al., 1997). Nevertheless, both afferent pathways input the SCN on its ventrolateral region. There remains, however, a possibility that dawn and dusk signals are equally received in the ventrolateral SCN, but there is a downstream switch that processes and transmits this information differently to the SCN network, depending on time of day.

In the dorsoventral plane of the mouse SCN, a photoperiod-dependent phase difference was recorded in PER2::LUC rhythms between the ventrolateral and dorsomedial regions (Evans et al., 2013). Photoperiod also modulates the spatiotemporal organization in clock gene rhythms in the anteroposterior plane (Inagaki et al., 2007; Yoshikawa et al., 2017). However, we find it hard to relate E-M to a binary subdivision of the SCN, since photoperiod affects not only the rhythms between the different subregions in a plane, but also within each subregion. As reviewed in Coomas et al (2015), the duration of nocturnal c-fos expression is longer in long nights versus short nights, both within the ventral and within the dorsal SCN. Also, Buijink et al., (2016) have recently shown a photoperiod-dependent change in the phase distribution within the anterior SCN.

Considering the difficulty in relating Model II to known physiological mechanisms, a more plausible configuration was tried in Model III, in which both E and M are sensitive to both dawn and dusk. However, in this configuration the two oscillators track the same pulse and **α** does not change at all under different photoperiods, regardless of oscillator asymmetries. It essentially resembles the behavior of a single oscillator in Model I. Model IV was an attempt to introduce a stereotyped asymmetry in the E and M responses, by inverting the sign of the light pulses to the M oscillator. This resulted in an inversion of the shape of its Phase Response Curve (Johnson, 1999) relative to the E oscillator. Although some changes in **α** were observed, the resulting patterns do not match experimental ones.

In sum, Model II best replicates experimental results but it requires two SCN subpopulations, each exclusively responsive to either dawn or dusk. While it still seems challenging to assign any of these features to the SCN and their light inputs, this model has a potential physiological counterpart at another step of photoperiod transduction beyond the SCN. As mentioned before, the SCN are the first step in a series of complex neuroendocrine pathways that regulate seasonal physiology, specifically seasonal reproduction (Nishiwaki-Ohkawa and Yoshimura, 2016; Wood and Loudon, 2014). In short, photoperiod-shaped neural outputs from the SCN control the nocturnal release of the pineal hormone melatonin, such that the duration of the melatonin signal matches the length of the night (Bartness et al., 1993). Melatonin information is, in turn, decoded in the *pars tuberalis* (PT) of the pituitary. Studies in sheep and hamsters suggest that, in the PT, the processing of melatonin duration depends on two events, the daily times of

melatonin rise and fall (Lincoln et al., 2003). Increasing melatonin levels at dusk control the phase of the clock gene *Cryptochrome1* (*Cry1*), whereas the decreasing melatonin levels at dawn control the phase of the clock gene *Period1* (*Per1*) (Lincoln et al., 2002; Messager et al., 2000; West et al., 2013). It has been proposed that the phase relationship between the two clock genes transduces the photoperiodic information to downstream molecular pathways, that ultimately regulate reproductive physiology (Lincoln, 2006; Lincoln et al., 2003). This mechanism is analogous to the "internal coincidence" model postulated long ago for photoperiod decoding (Pittendrigh, 1972). The molecular events in the PT are compatible with our E-M Model II, in which each oscillator is responsive to either dawn or dusk alone. Melatonin rise at dusk and melatonin fall at dawn are sensed by different oscillating molecules (*Cry1* and *Per1*), that are likely mutually regulated (coupled) in a molecular network (Lincoln, 2006; Lincoln et al., 2003). Alternatively, however, other mechanisms have also been proposed to explain the processing of the melatonin signal in the PT (Dardente and Cermakian, 2007; Masumoto et al., 2010).

In summary, in mammals there are two physiological steps in the decoding of photoperiodic information, which depend on the phase relationship between dawn and dusk events. The different working versions of the mathematical model could represent the decoding of daily light/dark proportion within the SCN or the transduction of the nocturnal melatonin signal duration within the PT. We found it challenging to quantitatively simulate a plausible E-M model that could match known physiological properties in the SCN and, at the same time, respond to photoperiod by promoting adjustments in **α** and psi-jumping at critical inter-pulse intervals. The models at which we arrived are overall approximations, each with its pros and cons. We hope this first approach can provide coordinating steps towards other ongoing modeling efforts.

ACKNOWLEDGEMENTS

We wish to thank W. Otto Friesen for the *Neurodynamix* software and Giovane C Improta for comments and suggestions to the manuscript. We thank the two anonymous referees for their very constructive criticisms. Funded by grants #2017/19680-2, 2017/16242-4, 2019/04451-3, São Paulo Research Foundation (FAPESP).

DECLARATION OF CONFLICTING INTERESTS

The Authors declares that there is no conflict of interest.

REFERENCES

Abrahamson E, and Moore RY (2001) Suprachiasmatic nucleus in the mouse: Retinal innervation, intrinsic organization and efferent projections. Brain Res 916:172–191.

Aschoff J (1966) Circadian activity pattern with two peaks. Ecology 47:657–662.

Baker JR (1938) The evolution of breeding seasons. In *Evolution, Essays on Aspects of Evolutionary Biology*, de Beer GR, ed, pp 161–177, Clarendon Press, Oxford, UK.

Bartness TJ, Powers JB, Hastings MH, Bittman EL, and Goldman BD (1993) The timed infusion paradigm for melatonin delivery: What has it taught us about the melatonin signal, its reception, and the photoperiodic control of seasonal responses? J Pineal Res 15:161–190.

Bennie JJ, Duffy JP, Inger R, and Gaston KJ (2014) Biogeography of time partitioning in mammals. Proc Natl Acad Sci 111:13727–13732.

Biello SM, Golombek DA, and Harrington ME (1997) Neuropeptide Y and glutamate block each other's phase shifts in the suprachiasmatic nucleus *in vitro*. Neuroscience 77(4):1049-57.

Borbély AA, Daan S, Wirz-Justice A, and Deboer T (2016) The two-process model of sleep regulation: A reappraisal. J Sleep Res 25:131–143.

Borbély AA, and Neuhaus HU (1978) Daily pattern of sleep, motor activity and feeding in the rat: Effects of regular and gradually extended photoperiods. J Comp Physiol A 124:1-14.

Boulos Z, and Macchi MM (2005) Season- and latitude-dependent effects of simulated twilights on circadian entrainment. J Biol Rhythms 20:132–144.

Bradshaw WE, and Holzapfel CM (2007) Evolution of animal photoperiodism. Annu Rev Ecol Evol Syst 38:1–25.

Brandstätter R, Kumar V, Abraham U, and Gwinner E (2000) Photoperiodic information acquired and stored *in vivo* is retained *in vitro* by a circadian oscillator, the avian pineal gland. Proc Natl Acad Sci 97:12324–12328.

Brown TM, and Piggins HD (2009) Spatiotemporal heterogeneity in the electrical activity of suprachiasmatic nuclei neurons and their response to photoperiod. J Biol Rhythms 24:44–54.

Buijink MR, Almog A, Wit CB, Roethler O, Olde Engberink AHO, Meijer JH, Garlaschelli D, Rohling JHT, and Michel S (2016) Evidence for weakened intercellular coupling in the mammalian circadian clock under long photoperiod. PLoS One 11:e0168954.

Ciarleglio CM, Axley JC, Strauss BR, Gamble KL, and McMahon DG (2011) Perinatal photoperiod imprints the circadian clock. Nat Neurosci 14(1):25-7.

Coomans CP, Ramkisoensing A, and Meijer JH (2015) The suprachiasmatic nuclei as a seasonal clock. Front Neuroendocrinol 37:29–42.

Daan S, and Aschoff J (1975) Circadian rhythms of locomotor activity in captive birds and mammals: Their variations with season and latitude. Oecologia 18:269–316.

Daan S, and Berde C (1978) Two coupled oscillators: Simulations of the circadian pacemaker in mammalian activity rhythms. J Theor Biol 70:297–313.

Daan S, Albrecht U, Van der Horst GTJ, Illnerova H, Roenneberg T, Wehr TA, and Schwartz WJ (2001) Assembling a clock for all seasons: Are there M and E oscillators in the genes? J Biol Rhythms 16:105–116.

Dardente H, and Cermakian N (2007) Molecular circadian rhythms in central and peripheral clocks in mammals. Chronobiol Int 24:195–213.

Deboer T (2018) Sleep homeostasis and the circadian clock: Do the circadian pacemaker and the sleep

homeostat influence each other's functioning? Neurobiol Sleep Circadian Rhythms 5:68–77.

DeCoursey PJ (1972) LD ratios and the entrainment of circadian activity in a nocturnal and a diurnal rodent. J Comp Physiol 78:221–235.

Edelstein K, and Amir S (1999) The Role of the Intergeniculate Leaflet in Entrainment of Circadian Rhythms to a Skeleton Photoperiod. J Neurosci 19(1):372-80.

Elliott JA (1976) Cicadian rhythms and photoperiodic time measurement in mammals. Fed Proc 35:2339–2346.

Elliott JA, and Tamarkin L (1994) Complex circadian regulation of pineal melatonin and wheel-running in Syrian hamsters. J Comp Physiol A 174:469–484.

Erkert HG (2000) Bats - Flying nocturnal mammals. In *Activity Patterns in Small Mammals*, S Halle and NC Stenseth, eds, pp 253–272, Springer-Verlag, Berlin.

Evans JA, Elliott JA, and Gorman MR (2004) Photoperiod differentially modulates photic and nonphotic phase response curves of hamsters. Am J Physiol Regul Integr Comp Physiol 286:R539–R546.

Evans JA, Leise TL, Castanon-Cervantes O, and Davidson AJ (2013) Dynamic interactions mediated by nonredundant signaling mechanisms couple circadian clock neurons. Neuron 80:973–983.

Farajnia S, van Westering TLE, Meijer JH, and Michel S (2014) Seasonal induction of GABAergic excitation in the central mammalian clock. Proc Natl Acad Sci 111:9627–9632.

Franken P, Tobler I, and Borbély AA (1995) Varying photoperiod in the laboratory rat: profound effect on 24-h sleep pattern but no effect on sleep homeostasis. Am J Physiol 269(3):R691-701.

Freeman DA, Dhandapani KM, and Goldman BD (2004) The thalamic intergeniculate leaflet modulates photoperiod responsiveness in Siberian hamsters. Brain Res 1028(1):31-8.

Friesen WO, and Friesen JA (1994) *NeuroDynamix : Computer-based neuronal models for neurophysiology*, Oxford University Press, New York.

Goldman BD (2001) Mammalian photoperiodic system: Formal properties and neuroendocrine

mechanisms of photoperiodic time measurement. J Biol Rhythms 16:283–301.

Gorman MR, Freeman DA, and Zucker I (1997) Photoperiodism in hamsters : Abrupt versus gradual changes in day length differentially entrain Morning and Evening circadian oscillators. J Biol Rhythms 12:122–135.

Harrington ME, Nance DM, Rusak B (1985) Neuropeptide Y immunoreactivity in the hamster geniculo-suprachiasmatic tract. Brain Res Bull 15(5):465-72.

Helfrich-Förster C (2009) Does the Morning and Evening oscillator model fit better for flies or mice? J Biol Rhythms 24:259–270.

Houben T, Deboer T, van Oosterhout F, and Meijer JH (2009) Correlation with behavioral activity and rest implies circadian regulation by SCN neuronal activity levels. J Biol Rhythms 24:477–487.

Ikegami K, and Yoshimura T (2012) Circadian clocks and the measurement of daylength in seasonal reproduction. Mol Cell Endocrinol. 349:76–81.

Illnerová H, and Vaněček J (1982) Two-oscillator structure of the pacemaker controlling the circadian rhythm of N-acetyltransferase in the rat pineal gland. J Comp Physiol A 145:539–548.

Inagaki N, Honma S, Ono D, Tanahashi Y, and Honma K (2007) Separate oscillating cell groups in mouse suprachiasmatic nucleus couple photoperiodically to the onset and end of daily activity. Proc Natl Acad Sci U. S. A. 104:7664–7669.

Jacob N, Vuilleza P, Lakdhar-Ghazalb N, and Pévet P (1999) Does the intergeniculate leaflet play a role in the integration of the photoperiod by the suprachiasmatic nucleus? Brain Res 828:83–90.

Jagota A, de la Iglesia H, and Schwartz WJ (2000) Morning and evening circadian oscillations in the suprachiasmatic nucleus *in vitro*. Nat Neurosci 3:372–376.

Johnson CH (1999) Forty Years of PRCs- What have we learned? Chronobiol Int 16:711–743.

Jones JR, Simon T, Lones L, Herzog ED (2018) SCN VIP neurons are essential for normal light-mediated resetting of the circadian system. J Neurosci 38(37):7986-7995.

Kawato M, and Suzuki R (1980) Two coupled neural oscillators as a model of the circadian pacemaker. J Theor Biol 86:547–575.

Kenagy GJ (1976) The periodicity of daily activity and its seasonal changes in free-ranging and captive kangaroo rats. Oecologia 24:105–140.

Kim HJ, and Harrington ME (2008) Neuropeptide Y-deficient mice show altered circadian response to simulated natural photoperiod. Brain Res 1246:96-100.

de la Iglesia HO, Meyer J, Carpino Jr. A, and Schwartz WJ (2000) Antiphase oscillation of the left and right suprachiasmatic nuclei. Science 290:799–801.

de la Iglesia HO, Fernandez-Duque E, Golombek DA, Lanza N, Duffy JF, Czeisler CA, and Valeggia CR (2015) Access to electric light is associated with shorter sleep duration in a traditionally hunter-gatherer community. J Biol Rhythms 30:342–350.

Lakin-Thomas PL, Brody S, and Coté GG (1991) Amplitude model for the effects of mutations and temperature on period and phase resetting of the Neurospora circadian oscillator. J Biol Rhythms 6:281–297.

Lincoln GA (2006) Decoding the nightly melatonin signal through circadian clockwork. Mol Cell Endocrinol 252:69–73.

Lincoln G, Messager S, Andersson H, and Hazlerigg D (2002) Temporal expression of seven clock genes in the suprachiasmatic nucleus and the *pars tuberalis* of the sheep: Evidence for an internal coincidence timer. Proc Natl Acad Sci 99:13890–13895.

Lincoln GA, Andersson H, and Loudon A (2003) Clock genes in calendar cells as the basis of annual timekeeping in mammals--a unifying hypothesis. J Endocrinol 179:1–13.

Lucassen EA, Diepen HC van, Houben T, Michel S, Colwell CS, and Meijer JH (2012) Role of vasoactive intestinal peptide in seasonal encoding by the suprachiasmatic nucleus clock. Eur J Neurosci 35:1466–1474.

Masumoto K, Ukai-Tadenuma M, Kasukawa T, Nagano M, Uno KD, Tsujino K, Horikawa K, Shigeyoshi Y, and Ueda HR (2010) Acute Induction of Eya3 by late-night light stimulation triggers TSHβ expression in photoperiodism. Curr Biol 20:2199–2206.

Menet J, Vuillez P, Jacob N, and Pevét P (2001) Intergeniculate leaflets lesion delays but does not prevent the integration of photoperiodic change by the suprachiasmatic nuclei. Brain Res 906:176-9.

Messager S, Hazlerigg DG, Mercer JG, and Morgan PJ (2000) Photoperiod differentially regulates the expression of Per1 and ICER in the *pars tuberalis* and the suprachiasmatic nucleus of the Siberian hamster. Eur J Neurosci 12:2865±2870.

Milette JJ, and Turek FW (1986) Circadian and photoperiodic effects of brief light pulses in male djungarian hamsters. Biol Reprod 35:327–335.

Mrugala M, Zlomanczuk P, Jagota A, and Schwartz WJ (2000) Rhythmic multiunit neural activity in slices of hamster suprachiasmatic nucleus reflect prior photoperiod. Am J Physiol Regul Integr Comp Physiol 278:R987-994.

Naito E, Watanabe T, Tei H, Yoshimura T, and Ebihara S (2008) Reorganization of the suprachiasmatic nucleus coding for day length. J Biol Rhythms 23:140–149.

Nishiwaki-Ohkawa T, and Yoshimura T (2016) Molecular basis for regulating seasonal reproduction in vertebrates. J Endocrinol 229:R117–127.

Nuesslein-Hildesheim B, O'Brien JA, Ebling FJ, Maywood ES, and Hastings MH (2000) The circadian cycle of mPER clock gene products in the suprachiasmatic nucleus of the siberian hamster encodes both daily and seasonal time. Eur J Neurosci 12:2856–2864.

Oda GA, and Friesen WO (2002) A model for "splitting" of running-wheel activity in hamsters. J Biol Rhythms 17:76–88.

Oda GA, and Friesen WO (2011) Modeling two-oscillator circadian systems entrained by two environmental cycles. PLoS One 6:e23895.

Oda GA, Menaker M, and Friesen WO (2000) Modeling the dual pacemaker system of the tau mutant hamster. J Biol Rhythms 15:246–264.

Pittendrigh CS (1972) Circadian surfaces and the diversity of possible roles of circadian organization in photoperiodic induction. Proc Natl Acad Sci USA. 69:2734–2737.

Pittendrigh CS (1981) Circadian organization and the photoperiodic phenomena. In *Biological Clocks in Seasonal Reproductive Cycles*, BK Follett, ed, pp 1–35, John Wright, Bristol.

Pittendrigh CS (1988) The photoperiodic phenomena: Seasonal modulation of the "day within." J Biol Rhythms 3:173–188.

Pittendrigh CS, and Daan S (1976a) A functional analysis of circadian pacemakers in nocturnal rodents: V. Pacemaker structure: A clock for all seasons. J Comp Physiol A 106:333–335.

Pittendrigh CS, and Daan S (1976b) A functional analysis of circadian pacemakers in nocturnal rodents: IV. Entrainment: Pacemaker as clock. J Comp Physiol A 106:291–331.

Pittendrigh CS, Kyner WT, and Takamura T (1991) The amplitude of circadian oscillations: Temperature dependence, latitudinal clines, and the photoperiodic time measurement. J Biol Rhythms 6:299–313.

Rohling J, Wolters L, and Meijer JH (2006) Simulation of day-length encoding in the SCN : From single-cell to tissue-level organization. J Biol Rhythms 21:301–313.

Schaap J, Albus H, vanderLeest HT, Eilers PHC, Détári L, and Meijer JH (2003) Heterogeneity of rhythmic suprachiasmatic nucleus neurons : Implications for circadian waveform and photoperiodic encoding. Proc Natl Acad Sci 100:15994–15999.

Schmal C, Myung J, Herzel H, and Bordyugov G (2015) A theoretical study on seasonality. Front Neurol 6:Article 94.

Schwartz WJ, de la Iglesia HO, Zlomanczuk P, and Illnerová H (2001) Encoding *le* quattro *stagioni* within the mammalian brain: Photoperiodic orchestration through the suprachiasmatic nucleus. J Biol Rhythms 16:302–311.

Shinohara K, Tominaga K, Isobe Y, and Inouye SI (1993) Photic regulation of peptides located in the ventrolateral subdivision of the suprachiasmatic nucleus of the rat: Daily variations of vasoactive intestinal polypeptide, gastrin-releasing peptide, and neuropeptide Y. J Neurosci 13(2):793-800.

Spoelstra K, Comas M, and Daan S (2014) Compression of daily activity time in mice lacking functional Per or Cry genes. Chronobiol Int 31:645–654.

Sumová A, Trávnícková Z, Peters R, Schwartz WJ, and Illnerová H (1995) The rat suprachiasmatic nucleus is a clock for all seasons. Proc Natl Acad Sci 92:7754–7758.

Tackenberg MC, and McMahon DG (2018) Photoperiodic programming of the SCN and its role in photoperiodic output. Neural Plast 8217345.

Takahashi JS, and Menaker M (1982) Entrainment of the circadian system of the house sparrow: A population of oscillators in pinealectomized birds. J Comp Physiol A 146:245–253.

Taylor SR, Wang TJ, Granados-Fuentes D, Herzog ED (2017). Resynchronization dynamics reveal that the ventral entrains the dorsal suprachiasmatic nucleus. J Biol Rhythms 32:35-47.

Trachsel L, Tobler I, and Borbély AA (1986) Sleep regulation in rats: Effects of sleep deprivation, light, and circadian phase. Am J Physiol 251(6):R1037-44.

Troein C, Locke JCW, Turner MS, and Millar AJ (2009) Weather and seasons together demand complex biological clocks. Curr Biol 19:1961–1964.

VanderLeest HT, Houben T, Michel S, Deboer T, Albus H, Vansteensel MJ, Block GD, and Meijer JH (2007) Seasonal encoding by the circadian pacemaker of the SCN. Curr Biol 17:468–473.

Wade GN, Bartness TJ, and Alexander JR (1986) Photoperiod and body weight in female Syrian hamsters: Skeleton photoperiods, response magnitude, and development of photorefractoriness. Physiol Behav 37:863–868.

Ware J V, Nelson OL, Robbins CT, and Jansen HT (2012) Temporal organization of activity in the brown bear (*Ursus arctos*): Roles of circadian rhythms, light, and food entrainment. Am J Physiol 303:R890-

902.

Wauters L, Swinnen C, and Dhondt AA (1992) Activity budget and foraging behaviour of red squirrels (*Sciuvus vulgaris*) in coniferous and deciduous habitats. J Zool London 227:71–86.

Weber ET, and Rea MA (1997) Neuropeptide Y blocks light-induced phase advances but not delays of the circadian activity rhythm in hamsters. Neurosci Lett 231(3):159-62.

West A, Dupré SM, Yu L, Paton IR, Miedzinska K, McNeilly AS, Davis JRE, Burt DW, and Loudon ASI (2013) Npas4 is activated by melatonin, and drives the clock gene Cry1 in the ovine *pars tuberalis.* Mol Endocrinol 27:979–989.

Williams CT, Barnes BM, and Buck CL (2012) Daily body temperature rhythms persist under the midnight sun but are absent during hibernation in free-living arctic ground squirrels. Biol Lett 8:31–34.

Wood S, and Loudon A (2014) Clocks for all seasons: Unwinding the roles and mechanisms of circadian and interval timers in the hypothalamus and pituitary. J Endocrinol 222:R39–R59.

Yetish G, Kaplan H, Gurven M, Wood B, Pontzer H, Manger PR, Wilson C, McGregor R, and Siegel JM (2015) Natural sleep and its seasonal variations in three pre-industrial societies. Curr Biol 25:2862–2868.

Yoshikawa T, Inagaki NF, Takagi S, Kuroda S, Yamazaki M, Watanabe M, Honma S, and Honma K (2017) Localization of photoperiod responsive circadian oscillators in the mouse suprachiasmatic nucleus. Sci Rep 7:1–13.

FIGURE LEGENDS

Figure 1. Examples from the literature, of activity patterns under varying photoperiods. (A) Double-plotted actogram depicting the nine-month activity record (black marks) of a nocturnal flying squirrel

(*Glaucomys volans*) exposed to natural, complete photoperiod variation schematized on top. Each line represents 48 hours of data and the vertical axis shows consecutive days, one below the other. Daily activity duration (**α**) parallels the length of the dark phase. (B) Double-plotted actogram depicting the activity record (black marks) of a mouse exposed to varying skeleton photoperiods, as schematized on top, in which 2 light pulses (white) occur daily on a darkness background (gray). The inter-pulse interval ("night" interval) that contains the activity phase is progressively shortened throughout the days. **α** is gradually compressed on days 140-180. Thereafter, the phase of entrainment is reversed to the complementary inter-pulse interval (psi-jump) and **α** is decompressed. (C) Phase of daily activity onset of hamsters (*Mesocricetus auratus*) exposed to different photoperiods. PPc: complete photoperiod. PPs: skeleton photoperiod. A: Daan and Aschoff, 1975; B: Spoelstra et al., 2011; C: Pittendrigh and Daan, 1976b. (A) Reprinted by permission from Springer Nature: Oecologia. Circadian rhythms of locomotor activity in captive birds and mammals: Their variations with season and latitude. Daan S and Achoff J, 1975. (B) Reprinted by permission from Taylor & Francis Ltd (http://www.tandfonline.com): Chronobiology International. Compression of daily activity time in mice lacking functional Per or Cry genes. Spoelstra K, Comas M and Daan S, 2014. (C) Reprinted by permission from Springer Nature: Journal of Comparative Physiology A: Neuroethology, Sensory, Neural, and Behavioral Physiology. A functional analysis of circadian pacemakers IV: Entrainment: Pacemaker as Clock. Pittendrigh CS and Daan S, 1976.

Figure 2. Conversion of oscillators state variables to daily activity/rest rhythms in the simulated animal. The process is illustrated for a 48-hour section of a simulation record. The oscillator is exposed to skeleton photoperiods indicated by "LD cycle" at the top, with white squares representing light pulses in a darkness (gray) background. The state variable *S* from the evening (S_E) and morning (S_M) oscillators are recorded continuously and compared to their activity thresholds. The peaks of the state variables are also recorded and represented as squares (evening) and triangles (morning). Whenever the state variables from both oscillators are below the threshold, the model animal is considered active, otherwise it is set as

inactive. This preliminary activity phase as well as the state variable peaks are represented by dashed symbols in the section "Activity (before 5h lag)". The pulses of the skeleton photoperiod are indicated as white squares. An addition step is made to better fit the phase to experimental data reported in the literature. We set a 5h lag (arrows) to the composite phases of oscillators and activity, relative to the light-dark cycle, as indicated in "Activity (after 5h lag)". The data for consecutive days is plotted one day below the other in the "Actogram". Each day represents 48 hours of data, with days 1-2 in the first line, 2-3 in the second line, and so forth. In the actogram, state variable peaks are only shown every 3 days to make visualization easier.

Figure 3. Four configurations of the model and their entrainment to different photoperiods. (A-D top) Schematic representation of model configurations depicting the skeleton photoperiods (gray-white bars), the oscillators (circular symbols) and the effects of the light pulses on the oscillators (arrows). When 2 oscillators are present (Models II-IV), curved arrows indicate coupling between them. (A-D bottom) Double-plotted actograms illustrating the activity rhythm of the model organism. Plotting conventions are the same used in Figure 2. (A) Model I – Single oscillator responsive to both pulses of the skeleton photoperiod. (B) Model II – Each oscillator is responsive to one of the pulses of the skeleton photoperiod. (C) Model III – E-M oscillators both respond to both pulses of the skeleton photoperiod. (D) Model IV – Same as previous model, except that the M oscillator receives pulses of negative amplitude (-), while the E oscillator receives regular pulses of positive amplitude (+). The days during the psi-jump are highlighted with a vertical line on the right of each actogram. (E-L) Phase of entrainment and activity duration of the four model configurations, under different skeleton photoperiods. Measurements were taken on the last day of exposure to each photoperiod, with stable entrainment of the activity rhythm. (E-H) Phase of entrainment. The times of activity onset and offset (black filled circles) are measured relative to the mid-point of the inter-pulse interval, in a circular scale (x axis). Onset and offset points are connected by a black dashed line. Diagonal white lines indicate the times of the pulses, as the skeleton photoperiod changes in the y axis. Peaks of the state variables are indicated for the evening (squares) and

morning (triangles) oscillators in each photoperiod. (I-L) Activity duration (**α**) under different photoperiods. Entrainment was not stable (missing points) at 12-hour "night" interval in E,H,I,L and at 10-hour "night" interval in F,G,J,K. In all versions of the model, oscillators have the standard configuration: a=0.85, b=0.3, c=0.8, d=0.5. Coupling is symmetric and positive ($C_{EM} = C_{ME} = 0.07$). Pulse duration: 1 hour; pulse amplitude: 1.1 or -1.1 (arbitrary units).

Figure 4. Effects of the coupling strength between E and M on the phase of entrainment, for Model II (Fig. 3B, top). Graphs are plotted following the same conventions of Figure 3E-H. (A-D) Different (symmetric) coupling strengths, as indicated above the graphs. Other model parameters as in Figure 3. Coupling determines how independently the phases of the oscillators change with different photoperiods. Coupling also affects the threshold photoperiod before the psi-jump.

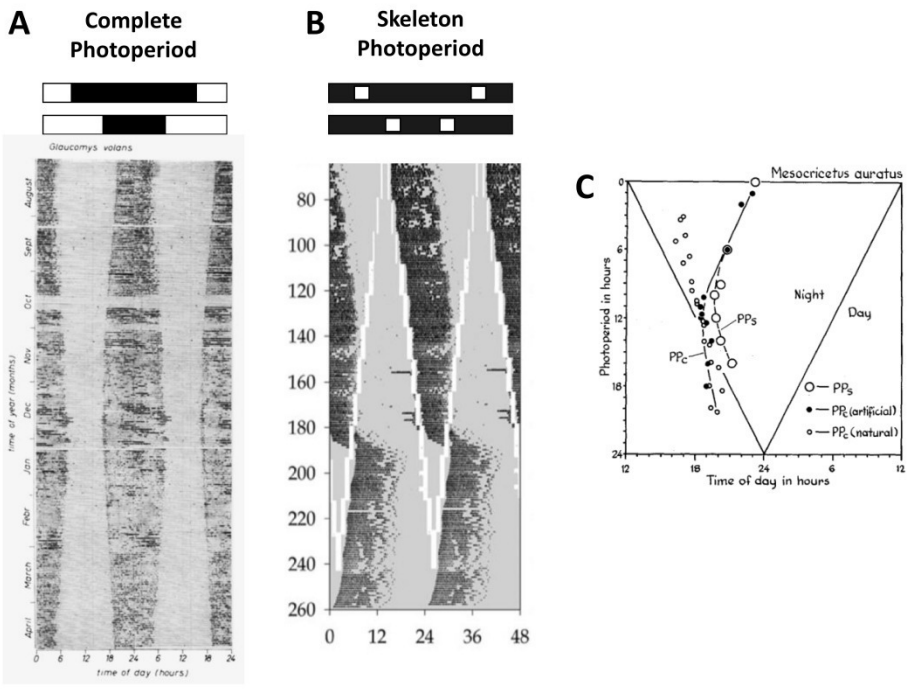

Figure 1. Examples from the literature, of activity patterns under varying photoperiods. (A) Double-plotted actogram depicting the nine-month activity record (black marks) of a nocturnal flying squirrel (*Glaucomys volans*) exposed to natural, complete photoperiod variation schematized on top. Each line represents 48 hours of data and the vertical axis shows consecutive days, one below the other. Daily activity duration (α) parallels the length of the dark phase. (B) Double-plotted actogram depicting the activity record (black marks) of a mouse exposed to varying skeleton photoperiods, as schematized on top, in which 2 light pulses (white) occur daily on a darkness background (gray). The inter-pulse interval ("night" interval) that contains the activity phase is progressively shortened throughout the days. α is gradually compressed on days 140-180. Thereafter, the phase of entrainment is reversed to the complementary inter-pulse interval (psi-jump) and α is decompressed. (C) Phase of daily activity onset of hamsters (*Mesocricetus auratus*) exposed to different photoperiods. PPc: complete photoperiod. PPs: skeleton photoperiod. A: Daan and Aschoff, 1975; B: Spoelstra et al., 2011; C: Pittendrigh and Daan, 1976b. (A) Reprinted by permission from Springer Nature: Oecologia. Circadian rhythms of locomotor activity in captive birds and mammals: Their variations with season and latitude. Daan S and Achoff J, 1975. (B) Reprinted by permission from Taylor & Francis Ltd (http://www.tandfonline.com): Chronobiology International. Compression of daily activity time in mice lacking functional Per or Cry genes. Spoelstra K, Comas M and Daan S, 2014. (C) Reprinted by permission from Springer Nature: Journal of Comparative Physiology A: Neuroethology, Sensory, Neural, and Behavioral Physiology. A functional analysis of circadian pacemakers IV: Entrainment: Pacemaker as Clock. Pittendrigh CS and Daan S, 1976.

173x136mm (800 x 800 DPI)

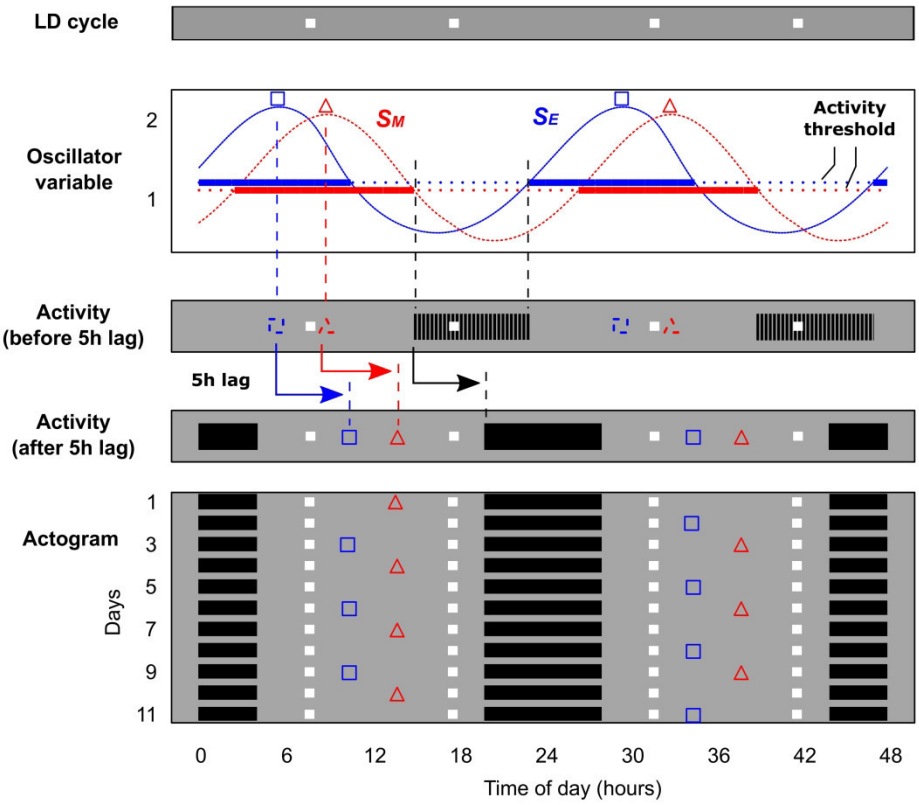

Figure 2. Conversion of oscillators state variables to daily activity/rest rhythms in the simulated animal. The process is illustrated for a 48-hour section of a simulation record. The oscillator is exposed to skeleton photoperiods indicated by "LD cycle" at the top, with white squares representing light pulses in a darkness (gray) background. The state variable S from the evening (S_E) and morning (S_M) oscillators are recorded continuously and compared to their activity thresholds. The peaks of the state variables are also recorded and represented as squares (evening) and triangles (morning). Whenever the state variables from both oscillators are below the threshold, the model animal is considered active, otherwise it is set as inactive. This preliminary activity phase as well as the state variable peaks are represented by dashed symbols in the section "Activity (before 5h lag)". The pulses of the skeleton photoperiod are indicated as white squares. An addition step is made to better fit the phase to experimental data reported in the literature. We set a 5h lag (arrows) to the composite phases of oscillators and activity, relative to the light-dark cycle, as indicated in "Activity (after 5h lag)". The data for consecutive days is plotted one day below the other in the "Actogram". Each day represents 48 hours of data, with days 1-2 in the first line, 2-3 in the second line, and so forth. In the actogram, state variable peaks are only shown every 3 days to make visualization easier.

173x157mm (600 x 600 DPI)

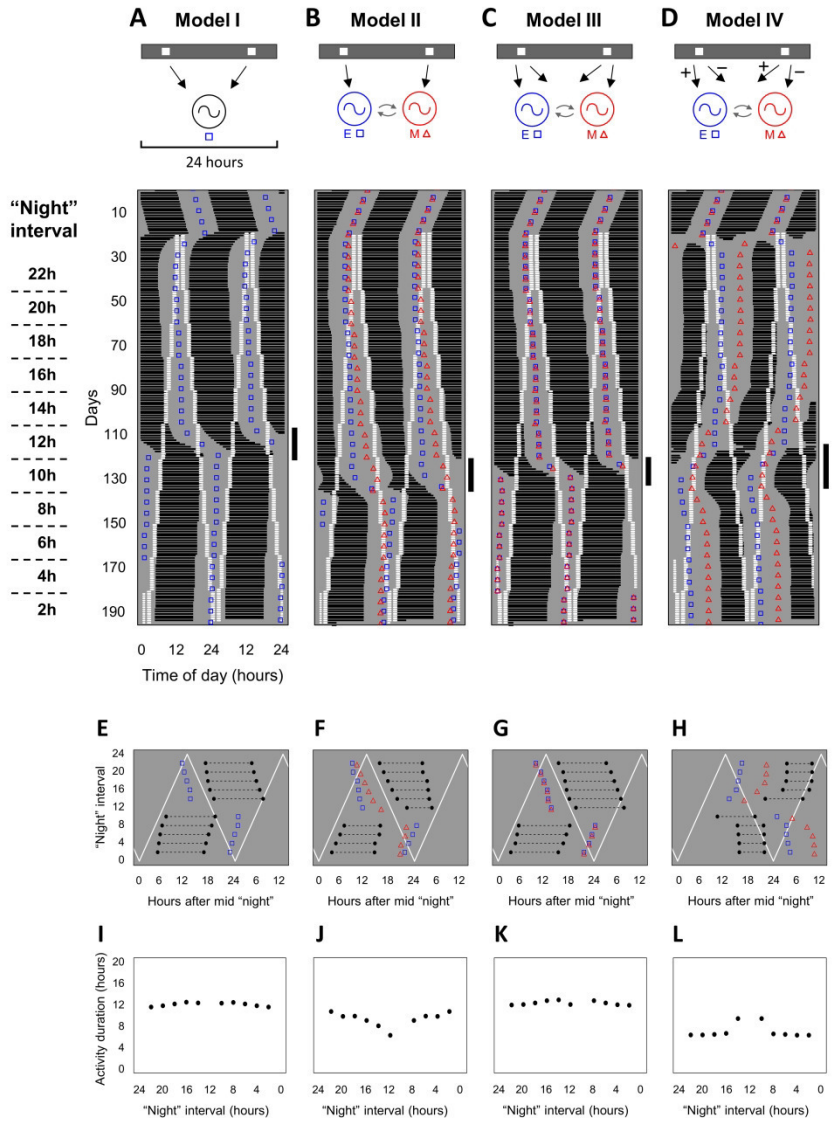

Figure 3. Four configurations of the model and their entrainment to different photoperiods. (A-D top) Schematic representation of model configurations depicting the skeleton photoperiods (gray-white bars), the oscillators (circular symbols) and the effects of the light pulses on the oscillators (arrows). When 2 oscillators are present (Models II-IV), curved arrows indicate coupling between them. (A-D bottom) Double-plotted actograms illustrating the activity rhythm of the model organism. Plotting conventions are the same used in Figure 2. (A) Model I – Single oscillator responsive to both pulses of the skeleton photoperiod. (B) Model II – Each oscillator is responsive to one of the pulses of the skeleton photoperiod. (C) Model III – E-M oscillators both respond to both pulses of the skeleton photoperiod. (D) Model IV – Same as previous model, except that the M oscillator receives pulses of negative amplitude (-), while the E oscillator receives regular pulses of positive amplitude (+). The days during the psi-jump are highlighted with a vertical line on the right of each actogram. (E-L) Phase of entrainment and activity duration of the four model configurations, under different skeleton photoperiods. Measurements were taken on the last day of exposure to each photoperiod, with stable entrainment of the activity rhythm. (E-H) Phase of entrainment. The times of activity onset and offset (black filled circles) are measured relative to the mid-point of the inter-pulse

interval, in a circular scale (x axis). Onset and offset points are connected by a black dashed line. Diagonal white lines indicate the times of the pulses, as the skeleton photoperiod changes in the y axis. Peaks of the state variables are indicated for the evening (squares) and morning (triangles) oscillators in each photoperiod. (I-L) Activity duration (α) under different photoperiods. Entrainment was not stable (missing points) at 12-hour "night" interval in E,H,I,L and at 10-hour "night" interval in F,G,J,K. In all versions of the model, oscillators have the standard configuration: a=0.85, b=0.3, c=0.8, d=0.5. Coupling is symmetric and positive (C_{EM} = C_{ME}=0.07). Pulse duration: 1 hour; pulse amplitude: 1.1 or -1.1 (arbitrary units).

173x233mm (600 x 600 DPI)

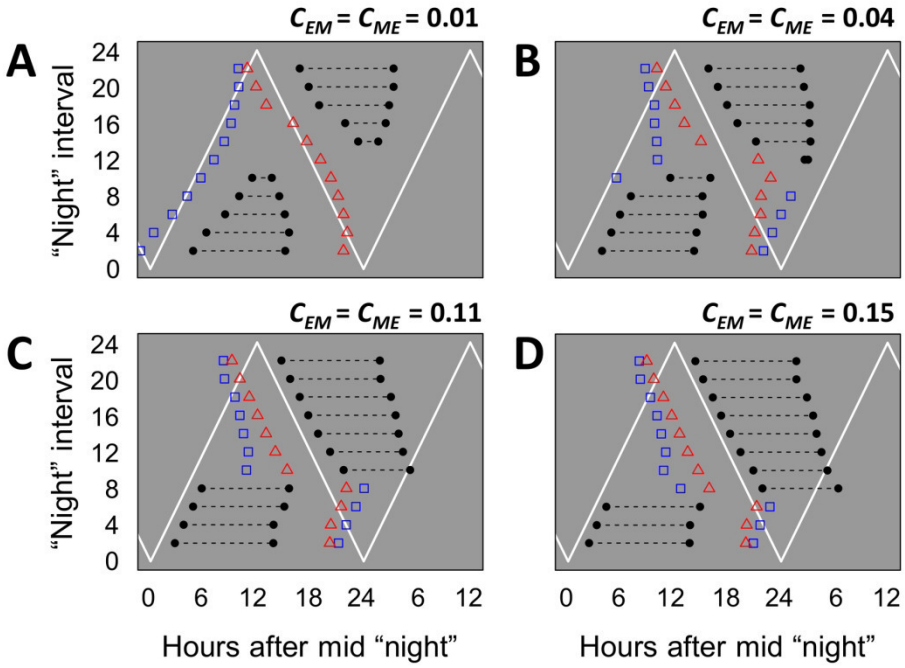

Figure 4. Effects of the coupling strength between E and M on the phase of entrainment, for Model II (Fig. 3B, top). Graphs are plotted following the same conventions of Figure 3E-H. (A-D) Different (symmetric) coupling strengths, as indicated above the graphs. Other model parameters as in Figure 3. Coupling determines how independently the phases of the oscillators change with different photoperiods. Coupling also affects the threshold photoperiod before the psi-jump.

82x63mm (600 x 600 DPI)

Supplemental Section

We describe below the attempts to find a Model III configuration (Fig. 3C) that displayed photoperiod-dependent changes in **α**. It has been shown previously that weakly coupled E and M with a phase difference can each respond with a different phase-shift, when subjected to a single pulse in constant conditions (Oda et al., 2000). This occurs because the pulse hits each oscillator in a different subjective phase. In this sense, we initially reasoned that, if E and M had a phase difference, light pulses of the skeleton photoperiod would hit each oscillator at different phases, generating more phase separation and consequent **α** changes. A non-null phase difference between oscillators can be obtained by asymmetries in oscillator configurations (Oda and Friesen, 2002). Thus, we replicated Model III with asymmetric E and M (Suppl. Fig. S2A, B). Interestingly, upon the start of the skeleton photoperiod, the pulses brought the oscillators closer together instead of separating them (Suppl. Fig. S2C). E and M moved together along different photoperiods, despite the great asymmetry in period and amplitude (Suppl. Fig. S2C,D). Consequently, **α** remained the same along different "night" intervals (Suppl. Fig. S2D).

This first variation of Model III failed to sustain and modulate the phase-difference between oscillators even with asymmetries. We hypothesized this could be explained because the two asymmetric oscillators, even when isolated, followed very similar patterns upon variations in the skeleton photoperiod (Suppl. Fig. S2E). Thus, we next aimed at finding E and M that tracked opposite pulses of the skeleton photoperiod when isolated. Our standard configuration tracks the "dusk" pulse (Fig. 3A), so we looked for configurations that tracked the "dawn" pulse. Together, the two coupled configurations could potentially rescue photoperiodic adjustments of **α** in Model III. Pittendrigh and Daan (1976) originally reported that the pulse to be tracked depends on the proportion between advances and delays in the Phase Response Curve (PRC) and on the free-running period of the oscillators. The standard configuration is expected to follow the dusk pulse because it has a greater proportion of delays in the PRC (Suppl. Fig. S8A) and its free-running period is longer than 24 hours. Therefore, we aimed at configurations with periods shorter than 24 hours and a greater proportion of advances in the PRC.

Several configurations were obtained by changing the four parameters *a*, *b*, *c* and *d*. We measured their free-running period and amplitude. Parameters were changed two-by-two at a time (six possible combinations) and results were plotted in six graphs representing the period-amplitude parameter space (Suppl. Fig. S3). For all configurations in one set (changes in *c* and *d*, "Δcd"), we also recorded the PRCs (Suppl. Fig. S4). From this partial exploration of the parameters space, we concluded that i) some parameter changes have a broad range of possible period-amplitude combinations, while others have narrower possibilities, and ii) combined changes in *c* and *d*, failed to arrive at PRCs with greater proportion of advances. From this latter

point, we gave up exploring oscillator PRCs and focused on the effects of the free-running period.

Using the parameter space in Supplemental Figure S3, we obtained fine-tuned oscillator configurations with different periods but iso-amplitude to the standard configuration (Suppl. Fig. S5A, "P" points; Table S1). When exposed to skeleton photoperiods, configurations with shorter period tended to follow the dawn pulse (Suppl. Fig. S5B). Of note, when the period diverges from 24 hours, the synchronization is lost for "night" intervals around 12 hours. These configurations were created by varying the *c* and *d* parameters but results were replicated with *b*-*c* and *b*-*d* (Suppl. Fig. S6). Changes in parameter *a* were not explored, since they allow fewer possibilities of period-amplitude values.

We found oscillator configurations (short-period) that follow the dawn pulse. If coupled to the standard configuration, we could supposedly create an E-M model and test for its photoperiodic-modulation in **α**. However, two asymmetric oscillators only display a stable, mutually synchronized rhythm if the period asymmetry is accompanied by amplitude asymmetry in the same direction (Oda and Friesen, 2002). Thus, we looked for configurations with modified amplitude, and a similar period compared to the standard configuration (Suppl. Fig. S5A, "A" points; Table S1). When exposed to skeleton photoperiods, configurations with different amplitudes follow the dusk pulse (Suppl. Fig. S5C). We also see a loss of synchronization at "night" intervals close to 12 hours, for oscillators with high amplitude.

Our main objective was to find a large-amplitude oscillator that still tracked the dusk pulse, so that it could be later coupled to a short-period oscillator that tracked the dawn pulse.

Having the iso-period and iso-amplitude configurations, we could compose a stable Model III configuration, with potential to present **α** modulation under different skeleton photoperiods. We combined a short-period-small-amplitude E, which in isolation follows the dawn pulse ("P3"), with a long-period-large-amplitude M, which in isolation follows the dusk pulse ("A3") (Suppl. Fig. S5A). The coupled E-M were exposed to skeleton photoperiods with both pulses delivered to both oscillators (Suppl. Fig. S7A). To our surprise, the oscillators did not separate, and instead both followed the dusk pulse (Suppl. Fig. S7C). Consequently, **α** again did not change in response to different photoperiods. We speculate that this is because M is a stronger oscillator, because of its larger intrinsic amplitude. Therefore, even though coupling is symmetric, the large-amplitude M has a stronger influence on the motion of the system than does the small-amplitude E. This hypothesis remains to be tested in future work as it would require an exhaustion of E-M combinations.

Altogether, we failed to compose a Model III with photoperiod-responsive **α** based solely on period and amplitude asymmetries. Neither could we test the role of the PRC, since all oscillator configurations present pronounced phase-delays compared to phase-advances. Thus, the predictions from Pittendrigh and Daan (1976) could not be tested by changing the oscillator

parameters. It occurred to us, however, that another non-intuitive strategy could be used to obtain PRCs with larger phase-advances. Pulses of negative amplitude should take the limit cycle to the opposite direction and could, therefore, invert the PRC. This was confirmed by building the PRC of the standard configuration in response to pulses of negative amplitude. The inverted PRC presented greater proportion of phase-advances (Suppl. Fig. S8B). Finally, we exposed the standard configuration to skeleton photoperiods with pulses of negative amplitude and, as expected, the oscillator followed the dawn pulse (Suppl. Fig. S8C). This strategy was used to build Model IV (Fig. 3D). In this model configuration, we applied negative pulses to the M oscillator and positive pulses to the E oscillator. Model IV is thus composed of two oscillators and each follows a different pulse of the skeleton photoperiod when isolated. This strategy is free from the confounding effects of oscillator amplitude asymmetries. Results with Model IV are discussed in the main text.

Table S1. Oscillator configurations used to test the effects of free-running period ("P") and amplitude ("A") on entrainment. Values of the four parameters (*a*, *b*, *c*, *d*) are given for each configuration.

Configuration	*a*	*b*	*c*	*d*
P1	0.85	0.30	1.15	1.05
P2	0.85	0.30	1.04	0.88
P3	0.85	0.30	0.95	0.75
P4	0.85	0.30	0.87	0.63
P5	0.85	0.30	0.74	0.44
P6	0.85	0.30	0.70	0.36
P7	0.85	0.30	0.64	0.29
P8	0.85	0.30	0.61	0.24
A0	0.85	0.30	1.12	0.35
A1	0.85	0.30	1.06	0.39
A2	0.85	0.30	0.51	0.52
A3	0.85	0.30	0.24	0.46
A4	0.85	0.30	0.05	0.37
xP1	0.85	0.42	0.80	0.83
xP3	0.85	0.36	0.80	0.65
xP6	0.85	0.26	0.80	0.42
xP8	0.85	0.22	0.80	0.34
xA1	0.85	0.45	0.80	0.28
xA3	0.85	0.17	0.80	0.97
xA4	0.85	0.14	0.80	1.22
yP1	0.85	0.62	0.27	0.50
yP3	0.85	0.45	0.55	0.50
yP6	0.85	0.21	0.93	0.50
yP8	0.85	0.12	1.07	0.50
yA1	0.85	0.14	1.34	0.50
yA3	0.85	0.29	0.29	0.50
yA4	0.85	0.27	0.16	0.50

Supplemental Figure legends

Figure S1. Photoperiod aftereffects on activity duration (α), in Model II configuration. Each line represents α recorded continuously on the last days of exposure to a skeleton photoperiod, and right after release in constant conditions (day 0, dotted line). The data for 3 different photoperiods is shown, with the "night" duration indicated next to each line.

Figure S2. Model III configuration with asymmetric E and M oscillators. (A) Schematic representation of the model configuration. Symbol correspondences as in Figure 3. (B) Free-running period and amplitude of different single-oscillator configurations (circles) obtained by changing parameter *a* (values indicated next to each circle). Other parameters were maintained in the standard values (*b*=0.3 *c*=0.8 *d*=0.5). The chosen E (blue) and M (red) oscillators are highlighted. (C) Activity of the asymmetric E-M model, initially free-running and later exposed to a skeleton photoperiod with 16-hour "night" interval. Plotting conventions as in Figures 2 and 3. (D) Phase of entrainment of the model under different skeleton photoperiods. Plotting conventions as in Figure 3. (E) Activities of isolated E (left) and M (right), exposed to varying skeleton photoperiods. Plotting conventions as in Figures 2 and 3.

Figure S3. Free-running period and amplitude of different single-oscillator configurations, obtained by changing parameters *a*, *b*, *c* and *d*. In each graph, two parameters were systematically changed (indicated on the top left), while the two others remained in the standard values (*a*=0.85, *b*=0.3, *c*=0.8, *d*=0.5). Orange and green lines in each graph connect configurations with changes in one of the two varying parameters, while the other remains constant. The value of the constant parameter for each line is indicated at one edge of the line.

Figure S4. Phase Response Curves (PRCs) of different single-oscillator configurations, given by different combinations of parameters *c* and *d*. PRCs were obtained by giving a single pulse to the free-running oscillator in constant conditions, at different circadian times (CT). The resulting phase-shift was measured after another 10 days, by comparing the new oscillator phase to the projected, unshifted free-running phase. Graphs show the phase-shift in the y axis as a function of pulse time in the x axis. Each graph has the PRCs for oscillators with the same value of parameter *c* (indicated on top) and varying values of parameter *d* (different colors explained in the top left graph).

Figure S5. Single-oscillator configurations with systematic changes in period or amplitude, obtained by adjusting parameters *c* and *d*. (A) Free-running period and amplitude of the different configurations (circles). Names given to each configuration are shown next to the gray circles. Parameter values are described in Table S1. The black circle in the middle is the standard oscillator configuration. Those starting with "P" indicate that the configuration has a different period, but the same amplitude as the standard configuration. Those stating with "A" have different amplitudes, but the same period as the standard configuration. (B) "P" configurations exposed to varying skeleton photoperiods, illustrating the effect of changes in free-running period on the entrainment under different photoperiods. (C) "A" configurations subjected to varying skeleton photoperiods, depicting the effect of different amplitudes on entrainment. Plotting conventions for B and C are the same used in previous actograms.

Figure S6. Replicate of systematic changes in single-oscillator amplitude and period, obtained by adjusting other equation parameters. (A and C) Free-running period and amplitude of the different oscillator configurations (circles), from adjustments in *b* and *d* (A), or *b* and *c* (C). Naming conventions were the same used in Figure S5, with the addition of a "x" (A) or a "y" (C) in front of the name. Parameter values are described in Table S1. (B and D) "xP" and "yP" configurations exposed to varying skeleton photoperiods illustrate the effects of oscillator free-running period on entrainment. Their overall behavior replicates the previous results in Figure S5, despite different parameter changes.

Figure S7. Model III configuration build with P3 (E) and A3 (M) oscillators, from Figure S5. When isolated, these oscillators track opposite pulses of the skeleton photoperiod (Suppl. Fig. S5). (A) Model scheme. Plotting conventions as in Figure 3. (B) Actogram depicting activity of the model, initially under free-running conditions and then exposed to a skeleton photoperiod with 16-hour "night" interval. Plotting conventions as in Figures 2 and 3. (C) Phase of entrainment of the model under different skeleton photoperiods. Plotting conventions as in Figure 3.

Figure S8. Oscillator response to pulses of negative amplitude. (A) Control Phase Response Curve (PRC) of the standard oscillator configuration exposed to pulses of positive amplitude. (B) PRC of the standard configuration subjected to pulses of negative amplitude. PRC protocol and plotting conventions are explained in Supplemental Figure S4. (C) Phase of entrainment of the standard oscillator configuration, under different skeleton photoperiods, with pulses of negative amplitude (scheme on top). Plotting conventions as in Figure 3.

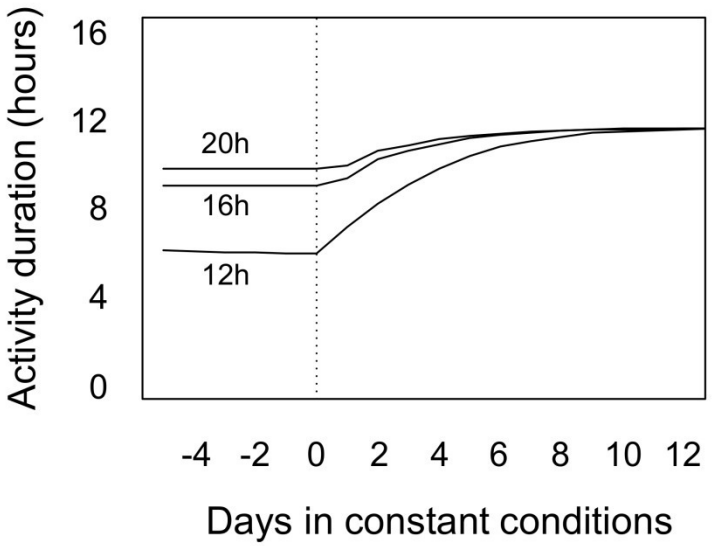

Figure S1. Photoperiod aftereffects on activity duration (α), in Model II configuration. Each line represents α recorded continuously on the last days of exposure to a skeleton photoperiod, and right after release in constant conditions (day 0, dotted line). The data for 3 different photoperiods is shown, with the "night" duration indicated next to each line.

82x62mm (800 x 800 DPI)

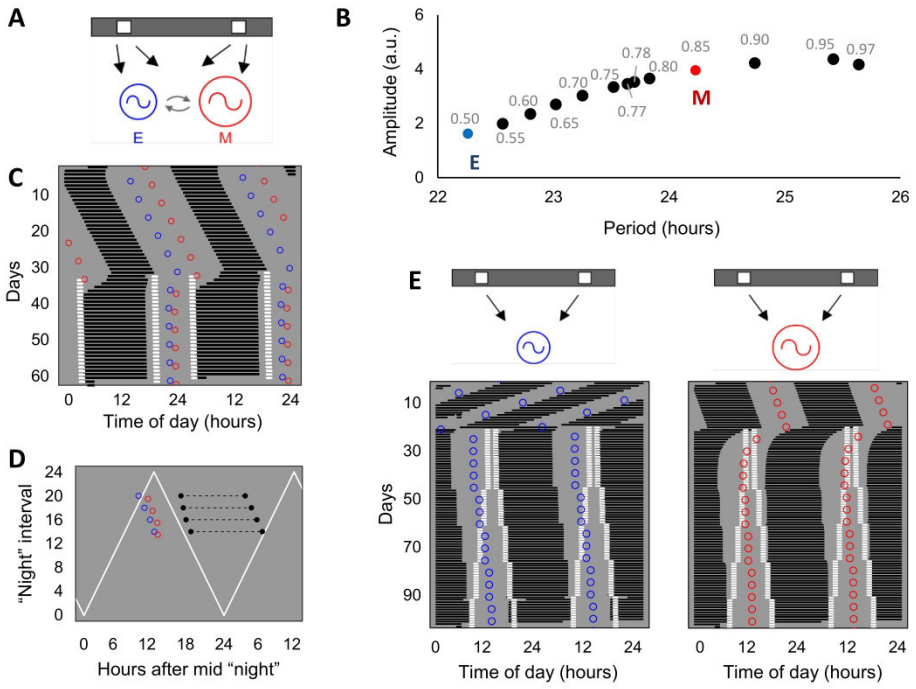

Figure S2. Model III configuration with asymmetric E and M oscillators. (A) Schematic representation of the model configuration. Symbol correspondences as in Figure 3. (B) Free-running period and amplitude of different single-oscillator configurations (circles) obtained by changing parameter a (values indicated next to each circle). Other parameters were maintained in the standard values (b=0.3 c=0.8 d=0.5). The chosen E (blue) and M (red) oscillators are highlighted. (C) Activity of the asymmetric E-M model, initially free-running and later exposed to a skeleton photoperiod with 16-hour "night" interval. Plotting conventions as in Figures 2 and 3. (D) Phase of entrainment of the model under different skeleton photoperiods. Plotting conventions as in Figure 3. (E) Activities of isolated E (left) and M (right), exposed to varying skeleton photoperiods. Plotting conventions as in Figures 2 and 3.

172x130mm (800 x 800 DPI)

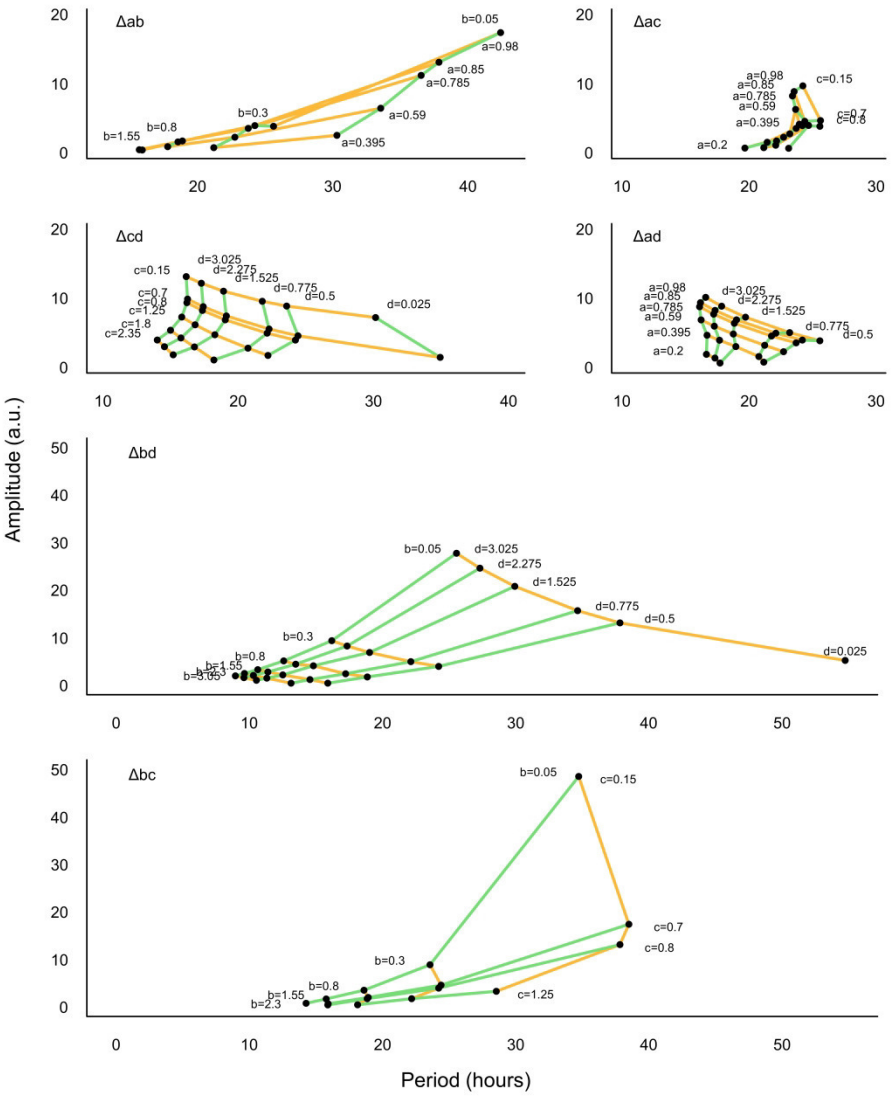

Figure S3. Free-running period and amplitude of different single-oscillator configurations, obtained by changing parameters*a*, *b*,*c* and *d*. In each graph, two parameters were systematically changed (indicated on the top left), while the two others remained in the standard values (*a*=0.85, *b*=0.3, *c*=0.8, *d*=0.5). Orange and green lines in each graph connect configurations with changes in one of the two varying parameters, while the other remains constant. The value of the constant parameter for each line is indicated at one edge of the line.

154x183mm (800 x 800 DPI)

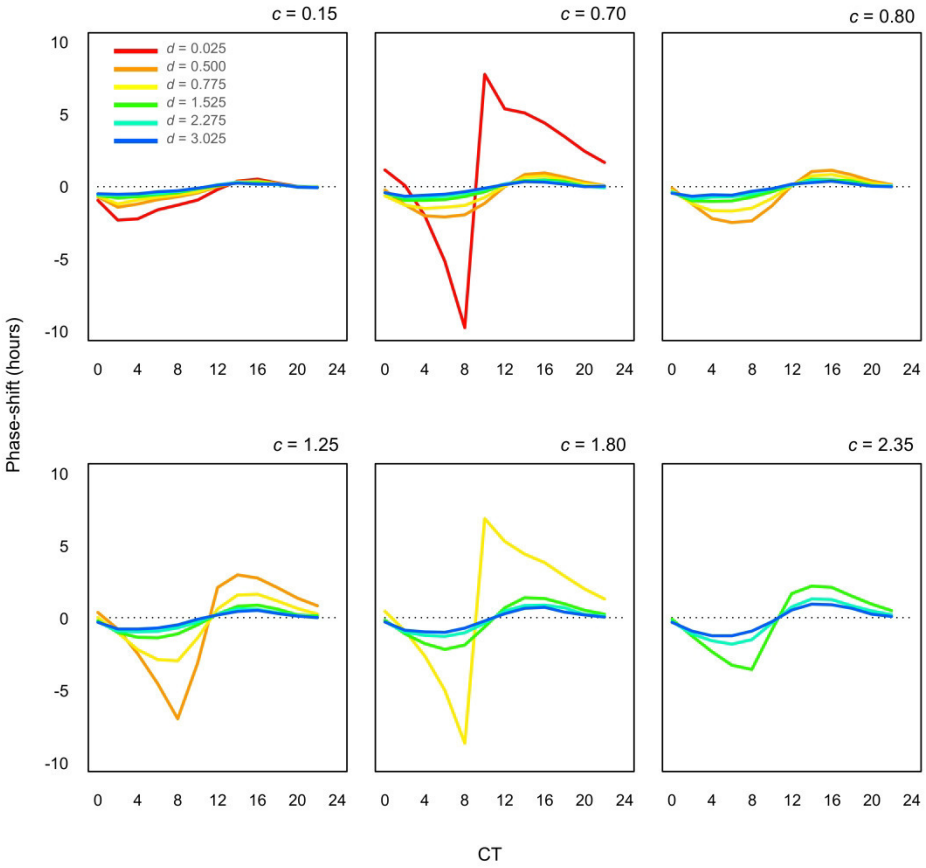

Figure S4. Phase Response Curves (PRCs) of different single-oscillator configurations, given by different combinations of parameters *c* and *d*. PRCs were obtained by giving a single pulse to the free-running oscillator in constant conditions, at different circadian times (CT). The resulting phase-shift was measured after another 10 days, by comparing the new oscillator phase to the projected, unshifted free-running phase. Graphs show the phase-shift in the y axis as a function of pulse time in the x axis. Each graph has the PRCs for oscillators with the same value of parameter *c* (indicated on top) and varying values of parameter *d* (different colors explained in the top left graph).

172x161mm (800 x 800 DPI)

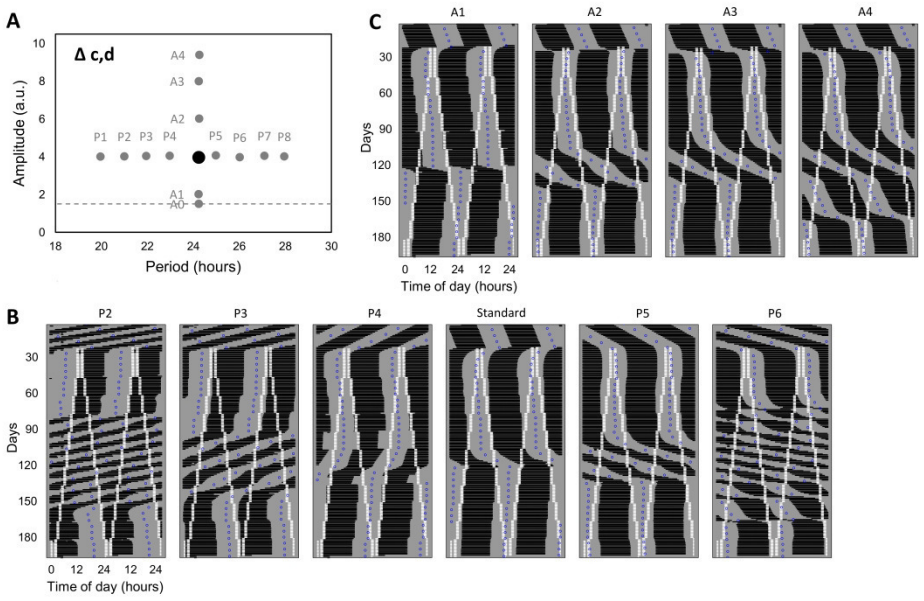

Figure S5. Single-oscillator configurations with systematic changes in period or amplitude, obtained by adjusting parameters *c* and *d*. (A) Free-running period and amplitude of the different configurations (circles). Names given to each configuration are shown next to the gray circles. Parameter values are described in Table S1. The black circle in the middle is the standard oscillator configuration. Those starting with "P" indicate that the configuration has a different period, but the same amplitude as the standard configuration. Those stating with "A" have different amplitudes, but the same period as the standard configuration. (B) "P" configurations exposed to varying skeleton photoperiods, illustrating the effect of changes in free-running period on the entrainment under different photoperiods. (C) "A" configurations subjected to varying skeleton photoperiods, depicting the effect of different amplitudes on entrainment. Plotting conventions for B and C are the same used in previous actograms.

210x135mm (800 x 800 DPI)

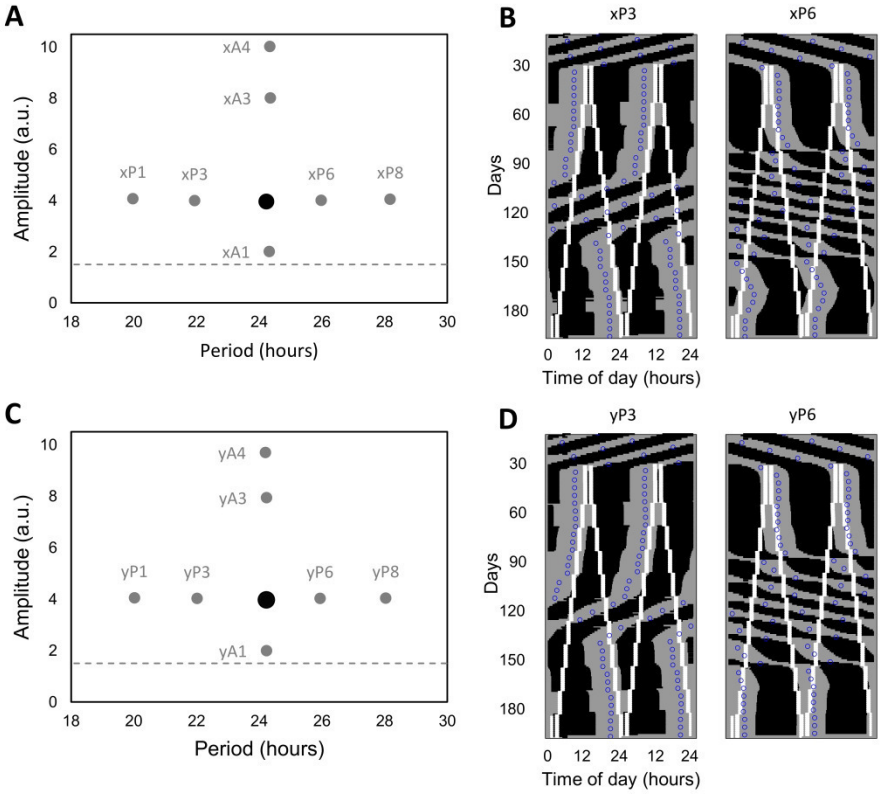

Figure S6. Replicate of systematic changes in single-oscillator amplitude and period, obtained by adjusting other equation parameters. (A and C) Free-running period and amplitude of the different oscillator configurations (circles), from adjustments in *b* and *d* (A), or *b* and *c* (C). Naming conventions were the same used in Figure S5, with the addition of a "x" (A) or a "y" (C) in front of the name. Parameter values are described in Table S1. (B and D) "xP" and "yP" configurations exposed to varying skeleton photoperiods illustrate the effects of oscillator free-running period on entrainment. Their overall behavior replicates the previous results in Figure S5, despite different parameter changes.

154x135mm (800 x 800 DPI)

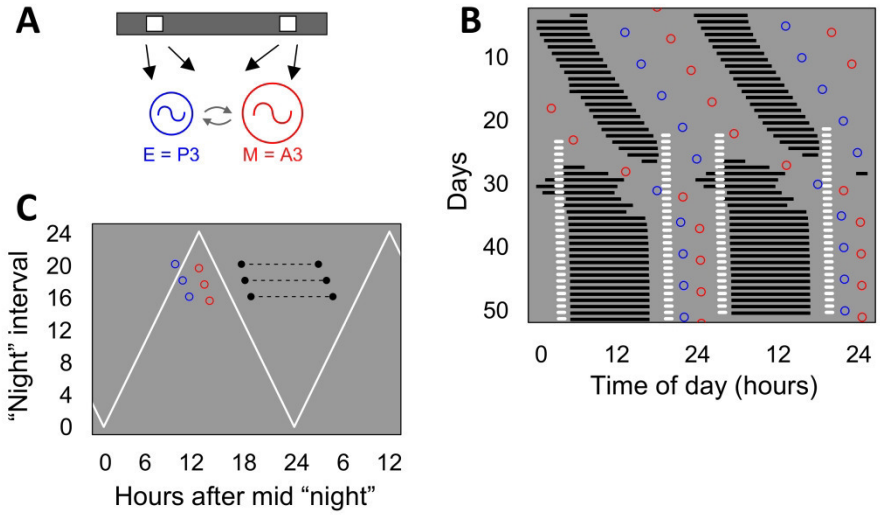

Figure S7. Model III configuration build with P3 (E) and A3 (M) oscillators, from Figure S5. When isolated, these oscillators track opposite pulses of the skeleton photoperiod (Suppl. Fig. S5). (A) Model scheme. Plotting conventions as in Figure 3. (B) Actogram depicting activity of the model, initially under free-running conditions and then exposed to a skeleton photoperiod with 16-hour "night" interval. Plotting conventions as in Figures 2 and 3. (C) Phase of entrainment of the model under different skeleton photoperiods. Plotting conventions as in Figure 3.

120x75mm (800 x 800 DPI)

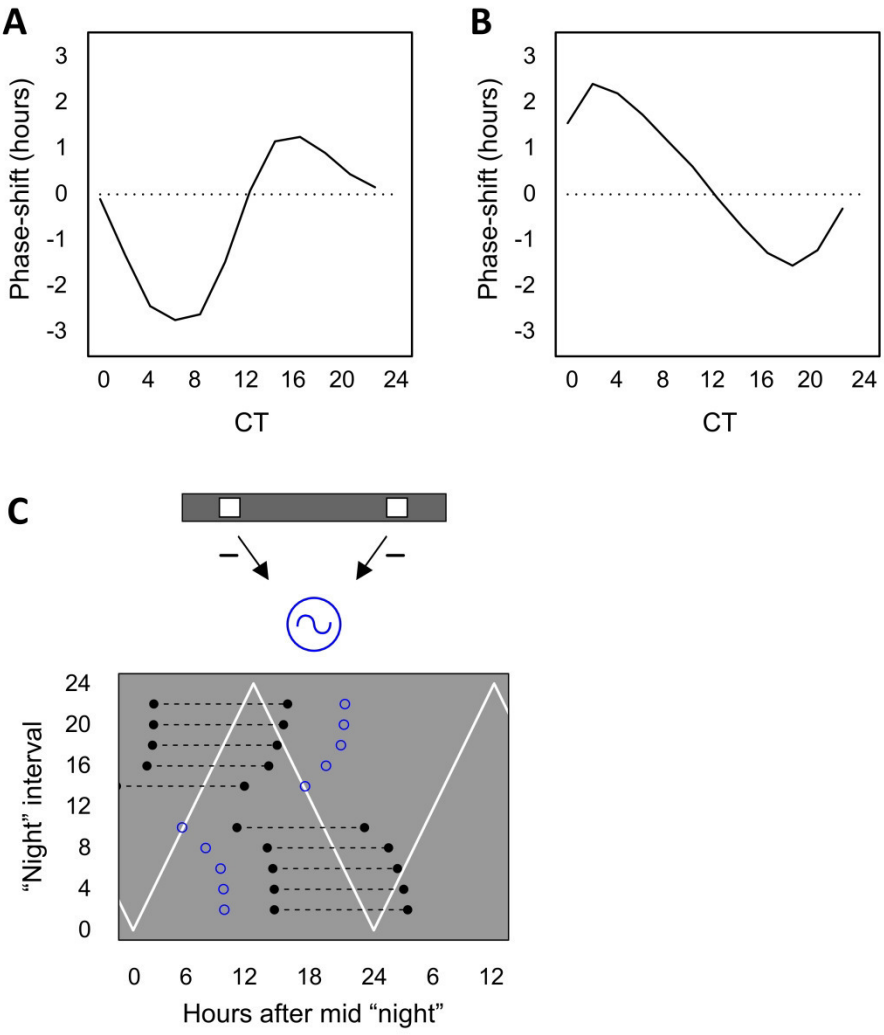

Figure S8. Oscillator response to pulses of negative amplitude. (A) Control Phase Response Curve (PRC) of the standard oscillator configuration exposed to pulses of positive amplitude. (B) PRC of the standard configuration subjected to pulses of negative amplitude. PRC protocol and plotting conventions are explained in Supplemental Figure S4. (C) Phase of entrainment of the standard oscillator configuration, under different skeleton photoperiods, with pulses of negative amplitude (scheme on top). Plotting conventions as in Figure 3.

120x136mm (800 x 800 DPI)